

In vivo multicell inferior olivary recordings: alternative design methods for creating cheap and flexible electrode structures

by

J.J. Kerpels

Technische Universiteit Delft



In vivo multicell inferior olivary recordings: alternative design methods for creating cheap and flexible electrode structures

by

J.J. Kerpels

to obtain the degree of Master of Science
at the Delft University of Technology,
to be defended publicly on Friday August 26, 2016 at 14:00.

Student number: 1307703
Thesis committee: Prof. dr. ir. W.A. Serdijn, TU Delft, supervisor
Prof. dr. P.J. French, TU Delft
M.J. Negrello PhD, Erasmus University Rotterdam

An electronic version of this thesis is available at <http://repository.tudelft.nl/>.

Preface

Where curiosity meets healthcare, things get interesting. The human brain has been a fascination for countless researchers in many fields of expertise, and for me as well. Although more and more is known about the brain, still so much remains a mystery. The natural urge for mankind to know everything there is to know can be combined with the necessity to understand the working of the human brain in order to prevent or cure certain nerve abnormalities. This is how this project got started. The focus of researchers at the Erasmus University of Rotterdam already had been on the olives for a while: two structures located in the brain stem which shows remarkable properties such as subthreshold oscillations and a very high density of so-called gap junctions. Since studies show that this structure may be closely related to complex movement coordination and learning motor tasks, it is of major interest to many researchers and clinicians.

During this project at Delft University of Technology, the ultimate goal we strived for was to create a wearable recording system with which we would be able to see neural activity of an animal when performing motor tasks, thereby hopefully confirming the theory. To do so, lightweight and cheap electrodes needed to be realized. This was the start of this project. A surface electrode was suggested by neuroscientists from Rotterdam. Although a nice design, results were a bit disappointing, since no clear signs of neural activity were found in the gathered data. Adjustments were made and the second version, which included microwire electrodes, was successful and action potentials were recorded. Since 3d-printing is hot and happening and promised a lot of design flexibility and robustness, and we were lucky enough to have such a complex machine for use at the Delft University of Technology, this possibility was investigated, which led to a new way of designing electrodes and fabricating them in-house rather than ordering expensive commercial products online. Wearable recordings were not achieved, but the new found methods could certainly lead to that.

This thesis was written in a chronological order. First, the background information was investigated to come to a first design. This design was then tested, and led to improvements. This knowledge led to the second design, and ultimately the third design. The designs were all evaluated on their own to create the next improved design, but since all designs had up- and downsides, the final chapter of this thesis reflects on all designs with respect to the requirements that were set beforehand and compares them to commercial products.

A lot of people were involved in making this work possible. First of all, most of the work was done together with Matthijs Weskin. We brainstormed on new design ideas and on how to solve the issues on designs afterwards. Secondly, a lot of people in the neuroscience lab in Rotterdam were involved, each of them in their own way. Mario and Jochen came up with the idea of the first electrode. Sander and Pascal helped with technical details such as exporting data and grinding electrodes. Vincenzo helped us using the measuring system in the lab. And finally Ruben, the neurosurgeon who allowed us to reach the structures of interest. His experience with the Olives from his PhD work helped all of us understanding and allowing what we were doing. Finally, some people in Delft were involved. Professor Wouter Serdijn and Vasiliki Giagka (Vasso) helped me in the creative process with their experience in both characterization and electrode design. Ide Swager, and his experience in 3d-printing, was responsible for me taking a look at that technique. Finally, Bram de Smit, from the faculty of Industrial Design, controls the 3d-printing facilities in their faculty. Together we worked towards a model with such small features, since that was never done before. I would really like to thank all of them for contributing to this work and allowing me to do such interesting research.

*J.J. Kerpels
Delft, August 2016*

Abstract

In order to allow neuroscientists to do in vivo recordings on hard to reach brain tissue, such as the inferior olivary complex, specially designed electrodes are required. Although a variety of electrodes are commercially available, they are usually expensive and it is hard to rapid prototype new designs. This thesis describes the design process of three electrode array designs, each improved based on the findings of the previous one. The first design was made using a FlexPCB production technique, on which gold spots were added to create conducting measuring sites. The second design combined this technique with commercial microwire electrodes. The third design used 3D print technology combined with microwire electrodes to create an electrode array. All designs were tested in in vivo measurements on mice. Successful measurements were carried out with the electrodes and the new production methods were found to be effective. Using a 3D printer to create electrodes makes for a very flexible design process and can be used to create very specific electrode shapes very rapidly and cost effective.

Contents

1	Introduction	1
2	Medical background and hypothesis	3
2.1	Cerebellum	3
2.2	Inferior olivary complex	4
2.2.1	Gap junctions	4
2.2.2	Action potentials	6
2.2.3	Subthreshold oscillations	7
3	Electrodes	9
3.1	Principle of electrodes	9
3.2	Currently available electrodes	10
3.2.1	Fabrication techniques	10
3.2.2	Commercial products	11
3.2.3	Experimental products	13
4	System requirements	15
4.1	Neuroscientific requirements	15
4.2	Engineering requirements	16
4.2.1	Electrode requirements	16
4.2.2	Measurement set-up requirements	17
5	First electrode design: FlexPCB	19
5.1	Existing setup and compatibility issues	19
5.2	Design	19
5.3	Characterization	22
5.3.1	Test signals	22
5.3.2	Impedance levels	25
5.4	In vivo measurements	29
5.5	Issues	31
6	Second electrode design: FlexPCB with tungsten tips	33
6.1	Design	33
6.2	Characterization	36
6.3	In vivo measurements	37
6.3.1	Unfiltered data	37
6.3.2	Filtered data	41
6.4	Issues	45
7	Third electrode design: 3D printed	47
7.1	First design	47
7.2	Printer characterization	48
7.2.1	Dimension tester	48
7.2.2	Cleaning process	49
7.2.3	Results	49
7.3	Second design	50
7.4	Characterization	52
7.5	In vivo measurements	55
7.5.1	Improved readout system	55
7.5.2	Unfiltered data	55
7.5.3	Filtered data	58
7.6	Issues	60

8	Conclusions and recommendations	61
8.1	Conclusions regarding requirements	61
8.2	New electrodes compared to commercial electrodes.	62
8.3	Recommendations	62
	Bibliography	65



Introduction

The brain has been a fascination for mankind ever since the ancient Egyptians wrote about it in the first medical document, now known as the *Edwin Smith Papyrus* written around 1600BC [1]. Research has been done extensively on how the brain functions and what parts are responsible for which function of the human body. Although a lot of information is gathered already in this field, most of the brain still remains a mystery. Since the brain is such a complex instrument, a lot can go wrong as well, leading to all kinds of malfunctioning conditions. Therefore, it is of vital importance that research keeps on being conducted to fully understand the working of the brain. The importance has been greatly underscored by the foundation of the *Brain Initiative* on April 2, 2013 by president Barack Obama. This initiative made a lot of money available and proposed a period over which researchers should enlarge their knowledge about the human brain, leading eventually to a full understanding of the brain.

Understanding how the brain works is arguably one of the greatest scientific challenges of our time.

Alivisatos et al. (2012) [2]

For students and researchers in the field of medicine, the brain offers a fascinating object of research. This is done via invasive and non invasive research. With invasive research a brain (usually of a guinea pig) is exposed in order to measure intracellular activity of the tissue. Examples for non invasive research are *EEG (electroencephalogram)*, where signals can be measured with electrodes outside of the skull and give valuable information on the brain activity. Or imaging methods such as *functional magnetic resonance imaging (fMRI)* can be used to map brain activity. Furthermore, secondary aspects can be investigated which give clues on the functioning or malfunctioning of the brain. Motor tasks and the learning of motor tasks for example can be used as a measure of the brain's well being. For students and researchers in the field of electrical engineering, the brain is fascinating as well, since the activity and communication in the brain and between the brain and the rest of the body is done in an electrical way. Charged ions flowing through gates in the cell membrane create potential differences, thereby creating action potentials that control everything in our bodies. Since the activity is all electrical, engineers can use electronics to both monitor and influence the signals in our brains.

The neuroscience lab of the Erasmus University of Rotterdam does research in a lot of fields involving the brain. Both non invasive research is done (motor tasks are being evaluated on a specialized device for mice) as well as invasive research, involving intracellular recordings on brain tissue. Both recording and stimulation is done, to see whether treatment can be realized by directly interacting with the brain. When investigating motor tasks, a lot of structures in the brain are found to be involved, but one structure in particular stands out: the *inferior olivary complex*. The axons arising from this structure form a major input to the *cerebellum*, or little brain, which is known to be responsible for posture and complex motor tasks. Since the cell bodies of the olives contain a high density of *Gap*

Junctions, directly connecting neighboring cells electrically, it is assumed that this structure realizes synchronization between signals and therefore allowing the brain to learn and perform complex motor tasks.

To create a deeper understanding, measurements were already done on the olives, but this is mostly done *in vitro*, using brain slices, or sometimes *in vivo*, but only on anesthetized animals. Since motor tasks are mostly suppressed in anesthetized animals, there is a strong wish to be able to monitor the olivary activity in wake animals. To do so, however, there is a need for small and light weight electrodes and electronics, which are currently not available in the lab in Rotterdam. And although the necessary equipment might be available commercially, it doesn't meet the requirements exactly, since these electrodes are not designed especially for the olive. Besides that, commercially available products are very expensive. Therefore, the research question of this project can be formulated as:

How can we use alternative production techniques to cheaply and reliably create structures for electrode arrays for in vivo multicell inferior olivary recordings?

To come to these in vivo measurements, a few steps need to be undertaken, not all of which will be discussed in this thesis. First of all, a small and lightweight electrode needs to be designed. Firstly, this will only be used on anesthetized animals, but the goal will be to ultimately wake the animal and perform readings when the animal does motor tasks, preferably with timing involved. Secondly, the readout system should be minimized. One possibility is to create a fully wearable system. Another possibility would be to create a wireless link between the animal and the readout electronics. The electronics will not be discussed in this thesis, since the electrode design is the main focus.

To come to a new electrode design, it is first of all important to evaluate the brain, and in particular the inferior olivary complex to create an understanding of what to expect during measurements. This is done in Chapter 2. The next chapter (Chapter 3) focuses on electrodes. It gives information as to what an electrode is, how to electrically model an electrode and shows electrodes currently commercially available. All this information combined with requirements set by neurologists in Rotterdam then leads to a set of requirements, discussed in Chapter 4. This then leads to the first electrode design, shown in Chapter 5, the second design in Chapter 6 and finally a third design in Chapter 7. Every design led to new knowledge and more understanding of how to design an electrode, and adjustments were made to improve each design. To sum up the goals reached and the issues that are still present in the latest design, the thesis concludes with Chapter 8: [Conclusions and recommendations](#).

A large part of this work was done in collaboration with Matthijs Weskin. The first and second electrode designs were created together. Matthijs was also involved in the assembling process of the third design electrode. Besides that, the measuring sessions were always done together. Matthijs focussed on the readout electronics while this work focussed on more electrode designs and the processing of the gathered data. The created readout system was then used with the third design electrode in the in vivo measurements. More information on his project can be found in his masters thesis [3].

2

Medical background and hypothesis

A human body is controlled via the *central nervous system*, or *CNS*. Different parts of this complex system take care of different processes of the body. A few large subdivisions can be distinguished in this CNS [4], also depicted in Figure 2.1:

- **The cerebrum** or the *big brain*
The largest part of the brain. This part is made up of two hemispheres and controls a lot of human actions, such as all voluntary movements, but also emotions and sensory inputs such as sound and vision.
- **The cerebellum** or the *little brain*
This structure is mainly involved in coordination of skeletal muscles, posture and balance.
- **The diencephalon**
The diencephalon consists of three major parts: the thalamus, hypothalamus and epithalamus, which are involved in producing hormones, secreting other materials and regulating things such as body temperature, hunger and thirst.
- **The brain stem**
The part of the CNS between the spinal cord and the diencephalon. Within the brain stem, a few structures can be observed, such as the medulla oblongata and the pons. The Olives are located within the medulla oblongata.
- **The spinal cord**
The spinal cord consists of nerves, mostly just the axons extending from the nervous cell bodies within other parts of the brain. This part is mainly to exchange information from the CNS to the rest of the body and vice versa.

For this research project, the main focus lies on the *olivocerebellar system*, which is formed by the cerebellum and the inferior olivary complex within the medulla oblongata in the brain stem. These structures are further investigated in Section 2.1 (cerebellum) and 2.2 (inferior olivary complex).

2.1. Cerebellum

The cerebellum is located underneath the cerebrum, and just behind the top part of the brain stem. Like the cerebrum, it has a folded structure. It takes up about 11% of the human brain, but a lot of nerve fibers are connected to the cerebellum or extend from the cerebellum. It is therefore an interesting region of the brain to investigate, since a lot of information is processed or created in this structure. A few basic functions are coordinated by the cerebellum [4]:

- **Movement**
The primary function of the cerebellum is evaluating movement. It monitors the movements initiated by the cerebrum and corrects these if necessary, by sending feedback to the motor areas of the cerebral cortex.

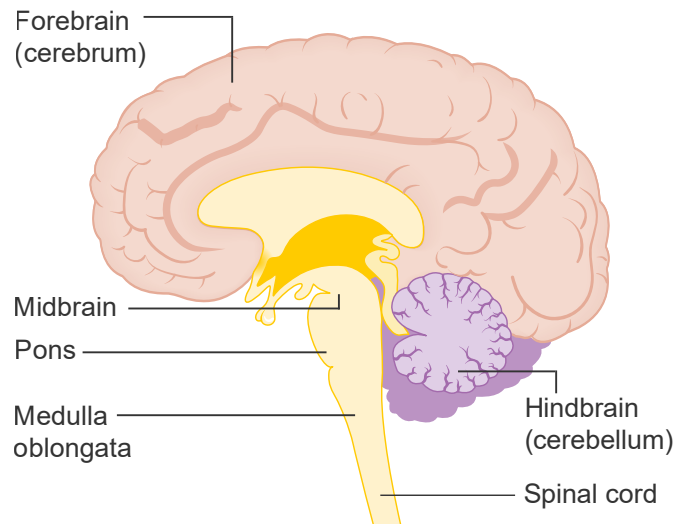


Figure 2.1: The main parts of the central nervous system in humans, saggital view.

By Cancer Research UK (Original email from CRUK) [CC BY-SA 4.0 (<http://creativecommons.org/licenses/by-sa/4.0>)], via Wikimedia Commons

- **Posture**

The cerebellum also coordinates complex and precise movements, and is thus heavily involved in posture and balance. Besides that, the precise muscle control by the cerebellum makes it that skilled actions can be carried out, such as catching a ball or speaking.

- **Cognition**

It is suggested that the little brain is also involved in cognition (the ability to acquire knowledge) and language processing. Studies using fMRI scans on subjects support this theory.

2.2. Inferior olivary complex

The inferior olivary complex is located in the brain stem, more precisely in the medulla oblongata. Figure 2.2 shows a detailed overview of where the structure is located inside the human brain. The oval shaped structures in this location are called the olives. The tissue here receives input from the cerebral cortex, the midbrain and the spinal cord. Neurons in the olives extend their axons mostly into the cerebellum, and form hereby a major source of input for the cerebellum [5][6]. These axons are commonly referred to as the *climbing fibers*. The neural signals coming from the olives influence the way the cerebellum controls the precise muscle activity and thus the olives play a major role in learning precise motor skills. The olivary cells have an oval shaped cell body of about 15 to 20 μm [7] and the olive itself has a triangular shape of 3 mm x 3 mm.

The next subsections will describe a few interesting aspects of the Inferior olivary complex. First of all, the *gap junctions* will be discussed in Subsection 2.2.1. Next, the typical *action potential* is explained in Subsection 2.2.2. Finally, the *subthreshold oscillations* that are typical for the olivary nervous signals will be discussed in Subsection 2.2.3.

2.2.1. Gap junctions

Nerve cells communicate with each other via chemical interfaces. Usually, this communication is done via the interaction between an axon and a dendrite with the use of neurotransmitters at synapses. An interesting difference between the olives and other areas of the brain is that the concentration of gap junctions is very high in the olives. Gap junctions are direct chemical connections between cells. They consist of a channel of 1.2 - 2 nm through which small ions and molecules can travel freely [8][9] called connexins. This way, cells can transfer neural signals directly from one cell to another, without the

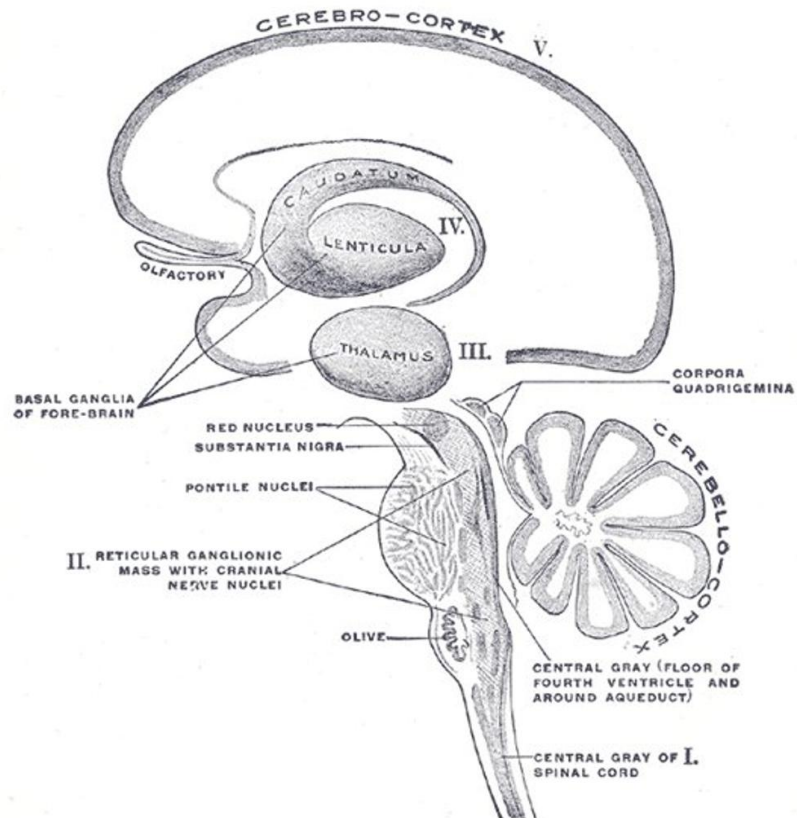


Figure 2.2: Saggital view of the human brain, olives are depicted in the lower part of the brain stem.
Case courtesy of Dr Jeremy Jones, Radiopaedia.org, rID: 36283

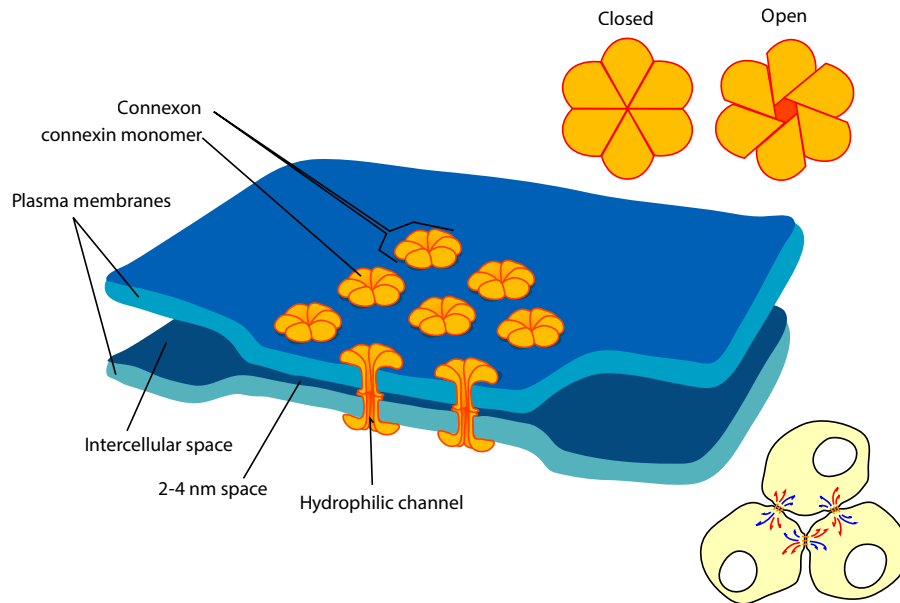


Figure 2.3: Schematic overview of a gap junction.
Image by Mariana Ruiz / Wikimedia Commons / Public Domain

need for a neurotransmitter. Because of this quick form of signal propagation, a lot of synchronization between cells can be performed [10]. Another location in the human body with a lot of gap junctions present is the heart muscle, where the synchronization of the signals are of vital importance to create the pumping action of the heart muscle [11]. A schematic overview of a gap junction is depicted in figure 2.3.

The combination of synchronizing temporal information and controlling precise muscle activity leads to the hypothesis that the olive is involved in synchronized activities, such as catching a ball. Some studies were done by Liu et al. to investigate this aspect. Subjects were given visual stimuli in a certain rhythmic pattern and were asked to detect any changes in this rhythm or changes in color or location of the object. Olivary action was only observed with a fMRI scan when the timing of the rhythm was changed, suggesting the olive to be part of the processing of temporal information [12][13].

2.2.2. Action potentials

Nerve cells require a certain amount of charge in order to be activated. The waveform generated when such a potential is reached, is called an *action potential*. Figure 2.4 gives an example of a typical action potential. A few different phases can be observed:

- **Depolarization phase**

When enough charge is built up in the nerve cell, the Na^+ channels open rapidly, causing a rapid change in membrane voltage because of a strong inflow of Na^+ ions.

- **Repolarization phase**

The slower K^+ channels open, causing positive charge to leave the cells. Simultaneously, the Na^+ channels close, causing less inflow of Na^+ , causing a net larger outflow of positive charges: the potential lowers again.

- **After-hyperpolarization phase**

The outflow of positive charges create a lower point than its resting potential, but returns to as the K^+ channels close.

- **Refractory period**

During this period, no build-up of charge can create an action potential, since all the channels are still closed.

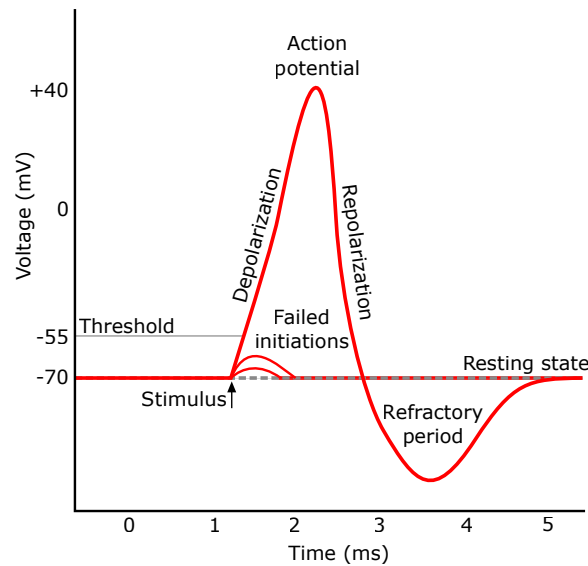


Figure 2.4: Typical waveform of an action potential.
 © Wikimedia Commons / CC-BY-SA-3.0 / GDFL

The values of such an action potential (such as duration of periods and potential levels) vary between different types of nerve cells. Olivary neurons typically show a latency to stimuli of about 15-30 ms before the action potential arises. When the threshold potential is reached, the depolarization phase shows a very steep peak, followed by an after-depolarizing phase. This phase lasts about 10-15 ms. After that, a long lasting after-hyperpolarization potential arises, which lasts around 150-200 ms. These action potentials are observed at a very low repetition frequency, only 1 or 2 per second. For research purposes, this can be altered chemically, but only to a maximum of about 8 to 10 Hz [7].

2.2.3. Subthreshold oscillations

Besides regular action potentials, the olivary membrane potentials oscillate at a low frequency. These oscillations are called *subthreshold oscillations*. These potentials are too low to invoke an action potential, hence the name *subthreshold*. In vitro, values of 4 - 10 Hz were observed at amplitudes of 3-10 mV. To investigate this property in an in vivo situation, and to analyze the synchronization properties of the gap junctions in relation to these oscillations, an electrode array needs to be designed, first to measure in anesthetized animals, but ultimately in awake animals.

3

Electrodes

As discussed in Chapter 2, a design of an electrode design is needed to be able to record in vivo neural signals from the olive in multiple locations simultaneously. To do so, it is important to know what an electrode is, how an electrode can be modeled electrically and what electrodes are already available for use commercially. This chapter firstly describes electrodes in general and models them (Section 3.1). Next, Subsection 3.2 focuses on currently available electrodes and how they are produced.

3.1. Principle of electrodes

Electrodes can be described as an instrument which forms the transducer between an *ionic current* inside an organism and an *electronic current*. They can be classified in two basic categories: recording electrodes create electric currents from ionic currents to be read out by electronics. This is done to observe signals inside an organism, such as brain signals (ECoG, EEG) or cardiac signals (ECG). The other way around, an electric current applied to an electrode can evoke an ionic current inside an organism, creating a stimulating electrode. Examples of such electrodes can be found as part of cardiac stimulating devices such as pacemakers or an Implantable Cardioverter -defibrillators (ICD's), but stimulating electrodes can also be found in deep brain stimulation or visual or cochlear prostheses. Since this project focuses on recording signals from brain tissue, this section focuses only on recording electrodes and how to model them.

To get to a model representing a single electrode, a few aspects of the interface between the tissue (or another conducting electrolyte) and the electrode need to be taken into account. When a conducting electrode is immersed in an electrolyte, both sides of the interface (electrolyte and electrode) get surrounded by a layer of charge, creating a so called *double layer*. This effect was firstly described by Hermann van Helmholtz in 1853. Charge is transferred from one side to another by two different mechanisms, *Faradaic* and *non-Faradaic* [14][15], which occur simultaneously.

- **Faradaic**

In the Faradaic, or resistive path of conduction, a process of oxidation and reduction causes charge to be exchanged between the two sides of the interface. This process can be modeled as a resistance (R_e) in the path from neural tissue to readout electronics.

- **Non-Faradaic**

In the non-Faradaic, or capacitive path of conduction, no actual charges are transferred between the electrode and the electrolyte, but the effect arises due to redistribution of charge on both sides of the interface. This can be electrically modelled as a capacitor (C_e).

To complete the model, the conductivity of the electrolyte can be modeled as a resistance in front of the electrode. This phenomenon is often called the *spreading resistance*, R_s , since this effect arises because of charges spreading out through the tissue or electrolyte. The ohmic resistance of the electrode can be modeled as a resistance as well (R_m). Since the material chosen to create the electrode usually

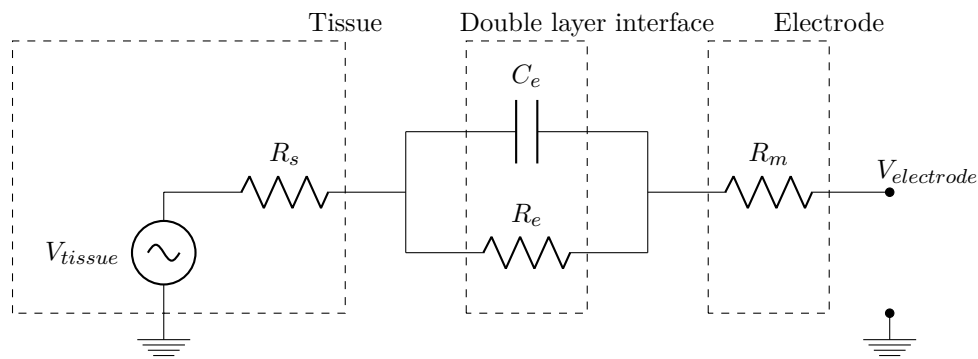


Figure 3.1: Electrical model of a recording electrode

has a high conductivity (and thus a low resistivity), this value is usually neglected when determining the impedance levels of an electrode. Last but not least, the ionic activity of the tissue is modeled as a voltage source (V_{tissue}), since potentials are to be recorded (such as action potentials). This all leads to the equivalent circuit shown in Figure 3.1, which gives an overview of the model with all these components.

3.2. Currently available electrodes

Various kinds of electrodes are widely available for all kinds of different applications. Depending on the application, designs differ in shape, size, material and fabrication technique. A few aspects to consider are:

- **Tissue type**
Target muscles or nerves (and central nervous system or periphery)
- **Invasiveness**
Surface electrodes or implantable electrodes
- **Duration**
Acute or chronic implantation
- **Electrode size**
Microelectrodes or macroelectrodes
- **Electrode structure**
Planar, cuffs or penetrating
- **Electrode material**
Rigid electrode or flexible electrode
- **Electrode peripherals**
Active or passive electrodes

The next subsections describe currently available products. First of all, different fabrication techniques are shown in Subsection 3.2.1, followed by a few commercially available products in Subsection 3.2.2.

3.2.1. Fabrication techniques

Listed below are a few production techniques currently used for producing microelectrodes and micro-electrode arrays. Each of the techniques is evaluated with positive (+) and negative (−) aspects.

- **Microwire** (such as shown in Figure 3.2)
 - + Well available and cheap
 - + Good mechanical performance (at least in longitudinal direction)
 - + Biocompatible materials are used (such as Tungsten conductors and Quartz isolators)
 - − Hard to handle because of size (micrometer scale diameters)

- **Silicon-based devices** (example in Figure 3.4a)
 - + High feature density
 - + Batch production makes it cheap
 - + Easy integration with electronics
 - + Si is considered biocompatible
 - Expensive to experiment with new designs
 - Stiff and rigid, so no way to follow tissue shape and high risk of tissue damage
- **Polymer-based devices**
 - + Flexible so compliant to tissue shape
 - + High tensile strength so robust during chronic implantation
 - + Biocompatible materials are used
 - No easy integration with electronics
 - Not much penetrative capabilities due to soft material
 - Higher moisture absorption compared to silicon-based devices
- **3D printed structures**
 - + Cheap to experiment with new designs
 - + Any shape is possible
 - + Biocompatible print material is available
 - Conductive print material is available, but the print resolution of that is very large (order of 1 mm)

3.2.2. Commercial products

Single electrodes

Single electrodes are available from a variety of companies, such as MicroProbes and Thomas Recording.

MicroProbes offers a big variety of single electrodes, varying in tip size and shape, conductor material and insulator material [16]. Shaft diameters varies from $81\ \mu\text{m}$ to $250\ \mu\text{m}$, with very sharp tips (down to $1\ \mu\text{m}$). The electrodes are sold preshaped and are provided with a connector to hook the electrode up to their readout system. An example of their single electrode is given in Figure 3.2a.

Thomas Recording provides the electrodes as raw material, meaning the electrodes are offered as a wire, which can be used to create an electrode using their specialized equipment [17]. This makes for very flexible electrode design in a research laboratory, since any tip shape can be created. An image is shown in Figure 3.2b, showing two grinded electrodes. The top electrode is just grinded, the bottom electrode is first heated en then pulled to create a sharper structure. After that, it gets grinded as well. Since these microwire electrodes are available for use in the laboratory in the neuroscience lab in Rotterdam, a detailed view is also given in Figure 3.3.

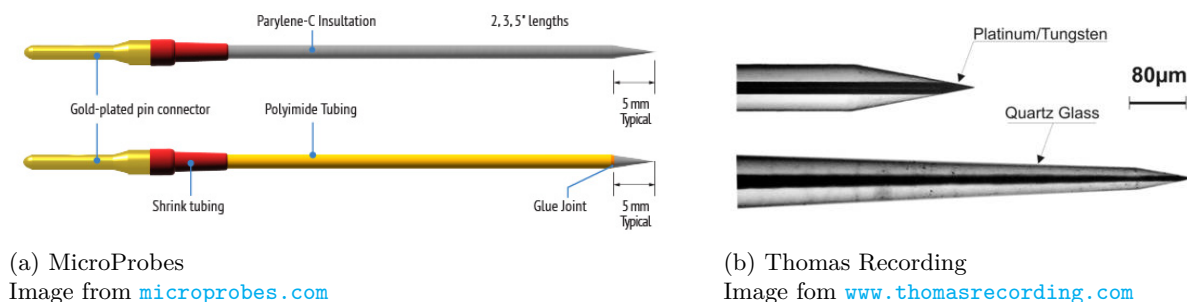


Figure 3.2: Some of the microwire single electrodes commercially available

Electrode arrays

Electrode arrays are capable of recording or stimulating in multiple locations at a time. Some of the commercially available electrode arrays are made out of microwire single electrodes as shown before, but other products provide a full electrode array as a package. A few commercial products are shown below.

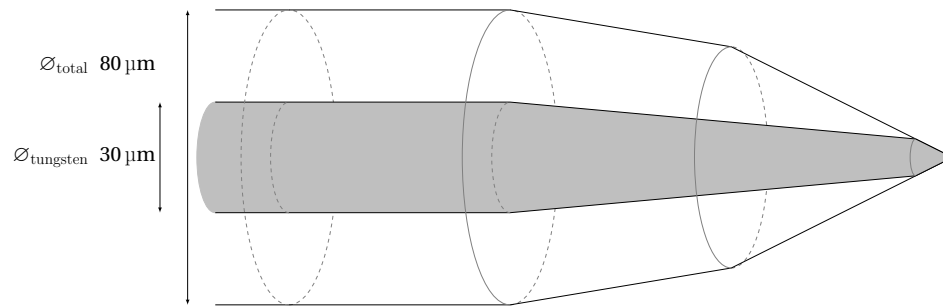


Figure 3.3: A schematic overview of the electrode tip of a Tungsten/Quartz electrode. The core is the Tungsten conductor, surrounded by a quartz insulation layer.

Utah array

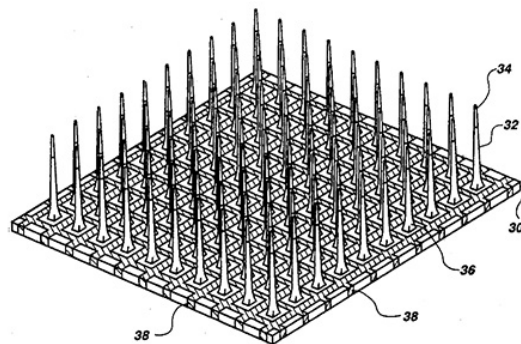
The Utah array is a high density silicon-based electrode array of 100 microneedles with a diameter of $80\ \mu\text{m}$ and a length of $1500\ \mu\text{m}$ and a pitch of $400\ \mu\text{m}$. The needles are insulated by glass. The tip of the needles are conducting, allowing for recording neural signals or stimulation. Figure 3.4a shows a schematic view of this electrode array.

Michigan Array

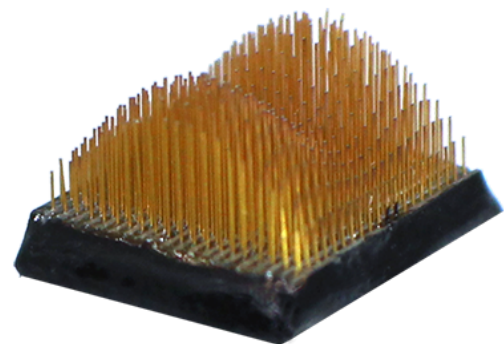
This silicon-based device is a 2-d structure, in contrast to the needles from the Utah array. It consists of one or more flat arms with conductive openings along the needle, creating measuring spots, so they allow for recording or stimulation along the shaft of each arm, rather than just the tip. This does provide higher spatial resolution than the Utah array.

Tucker Davis Technologies

Tucker Davis offers fully customizable electrode arrays. The number of electrodes can be adjusted, the length of the electrodes, the grinding of the electrode and the substrate can be chosen to be rigid or flexible. The electrodes themselves are microwire electrodes, but they come preassembled as a full electrode array including a connector to hook it up to readout systems. An example of a Tucker Davis electrode array is shown in Figure 3.4b.



(a) Utah Array



(b) Tucker Davis array

Figure 3.4: Two types of commercial electrode arrays.

Left (Figure 3.4a) the Utah Array, image by Richard A. Normann (US Patent #5,215,088) [Public domain], via Wikimedia Commons

Right (Figure 3.4b) a Tucker Davis electrode array. Image from www.tdt.com/cortical-arrays.html

Thomas Recording

The neuroscience lab in Rotterdam houses a Thomas Recording 32 electrode array. It consists of a large frame in which the microwire electrodes as shown in Figure 3.3 can be mounted. Each of these electrodes can then be individually moved in the longitudinal direction, making for very accurate placement of the electrodes. The system is however very large and requires the animal to be fixated and anesthetized in

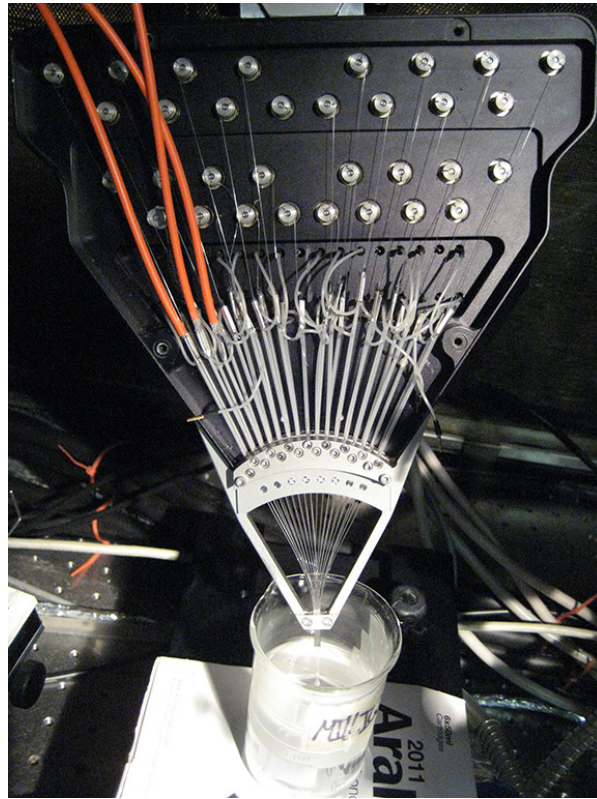


Figure 3.5: The Thomas Recording 32 channel electrode array

order to do measurements, which limits the possibilities of in vivo measurements. An image of the 32 electrode array is shown in Figure 3.5.

3.2.3. Experimental products

Whereas the Michigan and Utah array have been around for about 25 years now, still new development methods are being explored. In 2012, Salvo et al. used a 3D printer to create electrodes [18]. The structure consists of an array of needles with a tip diameter of $100\ \mu\text{m}$, with a pitch of $600\ \mu\text{m}$. The structure is printed with an acryl-based polymer. The structure is cleaned and dried, after which it is coated with gold in a vacuum coating chamber. This leads to an array with many needles, but they all form just one channel, with an enlarged surface area.

With the knowledge of the brain tissue to be investigated, the expected nervous signals to be recorded, and the currently available electrodes, a set of requirements can now be formulated. This will be done in Chapter 4.

4

System requirements¹

In Chapter 2 the waveforms present in the desired signal have been discussed. Based on these waveforms requirements of the measurement system can be obtained. Together with the neuroscientists of the Erasmus MC, Department of Neuroscience, a detailed set of system requirements from a neuroscientific point of view are set. These requirements are presented in the next section. A translation to requirements from an engineering point of view are presented in Section 4.2.

4.1. Neuroscientific requirements

In this section system requirements from a neuroscientific point of view are listed. All requirements are set in collaboration with the neuroscience department of the Erasmus MC. Some requirements are optional in this work, but must be kept in mind for future work. The origin of each requirement is explained shortly.

- **In vivo measurements**
All measurements are performed *in vivo*. To do so, the used electrodes must be *biocompatible* and the damage to the tissue must be minimized.
- **Measure sub-threshold and low-threshold oscillations**
Sub-threshold oscillations (STO, see Subsection 2.2.3) are present in the frequency band from 4 to 10 Hz. Low-threshold oscillations (LTO) in the band from 1 to 3 Hz.
- **Measure action potentials**
Action potentials (AP) contain frequencies up to *multiple kHz*, depending on the type of action potential. The repetition frequency of action potentials is *between 1 and 2 Hz*.
- **Measure propagation of oscillations and action potentials**
To reconstruct all waveforms (STO's, LTO's and AP's) a frequency range of *sub-Hz to multiple kHz* is necessary.
- **Number of electrodes**
There is *no restriction* on the number of electrodes used in the system. To measure spatially at least two electrodes are required.
- **Tissue and cell size**
Neural cells in the olivocerebellar system are oval shaped with a *diameter of 15 to 20 μm*. To record single cell potentials, electrode tips in the same order of magnitude must be used. The inferior olive is *triangular shaped, 3 by 3 mm* (see Subsection 2.2). The inserted electrodes must not exceed these dimensions.
- **Data processing**
Obtained data must be *displayed in real time* during the measurement to monitor the recording.

¹This chapter is partly co-authored by Matthijs Weskin

Besides displaying the data, it also must be *saved to a storage device* for extensive processing and analysing purposes. The data must be importable in Matlab and Spike2 (respectively engineering and neuroscience software).

- **Cheap**

Without losing signal quality the costs must be reduced. Existing set-ups containing expensive amplifiers, electrodes and accessories will limit the amount of set-ups and can reduce the number of measurements that can be performed, because just several set-ups are available. A new design must be cheaper than the existing measurement set-ups.

- **(Optional) Universal electronics**

The starting point for measurements is the olivocerebellar system, but with a different configuration of the set-up and perhaps another set of electrodes (depending on the location of the measurement and tissue properties), but without adding or changing electronic hardware, other brain signals also must be measurable.

- **(Optional) Wearable**

Initially the mice are anaesthetised during measurements, but a future goal is to measure in awake and freely moving mice. To realise these measurements, the used hardware must be wearable.

- **(Optional) Wireless**

When a set-up with awake mice is realised, a wireless link between the electronics on the mice, and a base station can be implemented. However, this is not in the scope of this thesis.

4.2. Engineering requirements

In the previous section the requirements from a neuroscientific perspective are listed. In this section the translation is made to an engineering point of view. To keep a clear overview, the requirements are split into the following subdesigns: electrodes, electronics and measurement set-up.

4.2.1. Electrode requirements

Specific requirements to the electrodes and the electrode array are listed in this subsection. The chosen values are based on the tissue properties (Chapter 2) and measurements with the existing set-up in the Erasmus MC.

- **Material**

The material for used electrodes or a base material for an electrode array must be biocompatible as it is implanted in an animal.

- **Electrode size**

Since the neural cells to measure have a diameter of 15 to 20 μm and single cell potentials must be measured, the electrode tip may not exceed the cell diameter: $\varnothing_{\text{tip}} 20 \mu\text{m}$.

The total electrode diameter may not damage the tissue significantly, therefore the maximum electrode diameter is set to five times the cell diameter: $\varnothing_{\text{electrode}} 100 \mu\text{m}$.

- **Array size**

The minimum number of electrodes in the array is not specified by neuroscientists, as long as the spatial and time resolution can be met. The physical size of the array on the other hand is limited to the size of the inferior olive: a triangle of 3 by 3 mm.

- **Connection**

The system can work *stand-alone*, but to test the electrode array on itself a connection to the existing set-up in the Erasmus MC is required.

- **Impedance**

The small voltage potential from the source needs a large amplification. The higher the impedance of the electrode, the higher the input impedance of the amplifier has to be. Ideally the impedance of the electrode is zero, but with the small sizes this is fairly impossible. To quantify this measure, the impedance of the existing micro-electrodes is chosen: $Z_{\text{electrode}} \leq 1 \text{ M}\Omega$ at 1 kHz.

4.2.2. Measurement set-up requirements

The existing measurement set-up is large and used for different purposes without optimising it to a specific measurement. In this subsection requirements on a new set-up are presented. Besides the design of a new set-up, the existing set-up must be updated and improved.

- **Size**
Initially the measurement system can be any size, but with an eye on the future, it must be taken into account that the system must become wearable and wireless. No restriction in size is chosen, but the possibility of reducing the size must be investigated.
- **Electromagnetic interference (EMI)**
Electromagnetic interference (EMI) may not dominate the measured signal. Especially interference inside the bandwidth (e.g. 50Hz-interference from the mains) must be suppressed.

In the next Chapters the design is explained, following the system requirements set in this Chapter. Additional requirements to sub-designs following from the above listed requirements, are discussed in the corresponding chapters. All requirements are evaluated in Chapter 8, [Conclusions and recommendations](#). Improvements are proposed for requirements that are not met.

5

First electrode design: FlexPCB

Measuring signals from the olivary complex requires a very specific measuring device, especially when multiple cells are to be recorded at once. Since the signals are proposed to have a relation to temporal information, there is a strong need to be able to do measurements *in vivo*: in a live animal. Previous research showed particular activity of the olive when performing timing related tasks, so it is desirable to create an environment in which the animal is experiencing time related events. For practical reasons the decision was made to record olivary signals from mice. Although the brain of mice is relatively small compared to other animals, making it harder to reach the specific tissue of the olive, it is legally more practical to choose mice for the research.

The design of the first measuring electrode consisted of a few steps, leading to the first set of measurements. First of all, some parts of the measurement setup were already available, creating both an advantage and a disadvantage. Although not every part of the measuring setup needs to be designed especially for this experiment, the parts that are newly designed for this purpose need to be compatible with the current setup. This is described in Section 5.1. After the analysis of the compatibility issues, the specifications of the design need to be formulated, such as size, distance between electrodes and materials. With this information available, the process of designing the first electrode could start (Section 5.2). After that, the device is characterized (Section 5.3) and used in an *in vivo* measurement (Section 5.4). Finally, some issues regarding the structural design are addressed in Section 5.5.

5.1. Existing setup and compatibility issues

The main focus at this stage of the analysis of the measurement setup is the issue of designing a device that is compatible with the setup. Although it is very important to know more specifications of the setup, such as gain and noise levels, the decision was made to only analyze the setup for practical issues at this stage of the design process. The two main issues here were the maximum number of connections, and the types of connection used by the setup. A 32-channel electrode array and preamplifier by Thomas Recording was present in the current setup, limiting the number of channels on the device to be designed to 32. The 32 measuring channels are connected to the head stage by specific gold male connectors which were available to be incorporated on the new device, making it possible to directly plug the device to the head stage. The ground of the system was available through a banana plug. The head stage samples the received signal with a sampling frequency of 24414 Hz before converting the signal to the optical domain. This signal is optically connected to a computer system, thus avoiding further electromagnetic interference.

5.2. Design

The shape of the olive leads to the first specification of the first electrode design. The olive consists of two parts (part of the left and right hemisphere of the brain), combining to a semi oval shape. The choice was made to focus on one half of the structure, resulting in a more or less triangular shape, with sides of 3 mm. Figure 5.1 depicts the situation.

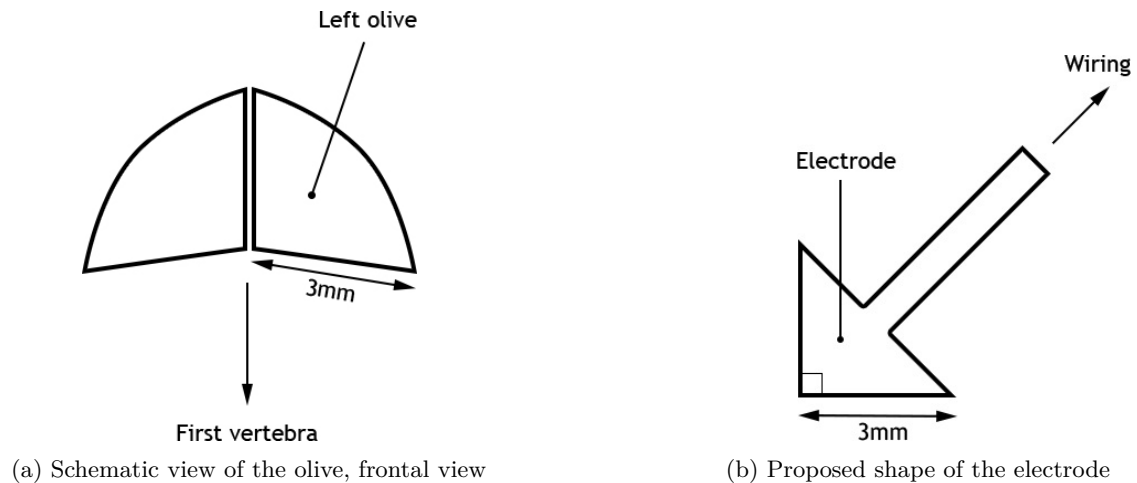


Figure 5.1: Specifications regarding shape and size of the electrode

The inferior olive is located in the medulla oblongata, a structure located just above the first vertebra, in the lower portion of the brain stem, in front of the cerebellum (from a frontal perspective). This region is hard to reach, especially when it is essential for the measurement that the animal keeps functioning normally. A frontal approach was suggested by the participating surgeon. This meant reaching the olive via the front size of the neck of the animal, carefully bypassing the trachea and esophagus. This procedure requires to bypass a lot of structures, so a rigid design could make it extra complicated to reach the structure. A flexible material was chosen to create the design.

Now that the specifications of the shape and size are clear, the next step is to decide on the measuring spots, the array size and the number of electrodes. The measurements are focused on timing differences between cells of the olive, so the distance between electrodes should ideally be small enough to be able to observe the same signal propagate, but big enough to ensure seeing time differences. To make sure the potential of single cells is recorded on a single measuring spot, a single measuring spot is ideally very small, in the range of an olivary nuclear body (about 15-20 μm [7]).

The signal measured at the tip of the electrode needs to travel from the electrode to the exterior environment. This part passes other neural or otherwise electrically active structures along the way (such as veins or the trachea). To lower the amount of influence these signals will have on the measured signal, it might be beneficial to create an extra metal layer within the electrode. Table 5.1 summarizes the specifications listed in this section.

Table 5.1: Specifications of first electrode design

Specification	
Connections	Measuring channels: male golden pins Ground: banana plug
Shape	Triangular, small wiring to outside
Total size	Rectangular triangle with sides of 3mm
Size of measuring spots	15 - 20 μm
Material	Flexible
Shielding	Extra metal layer

Now that the specifications of the design have been formulated, a conceptual design was made. Because of production limitations, not all of the specifications could be reached. The main limitations proved to be the line width, the line spacing. and the via size. The line width gives the minimum size a connecting path should be, the line spacing how much space is minimally required between these paths. The via size gives the minimum size needed to create a via: a connection from one conductive layer to another. These three limitations lead to the decision to create an electrode with 10 channels, since this would be the maximum number to create on the triangular size while still having room for the via's. The signals

paths are divided into two conductive signal layers, all created on a flexible printed circuit board, with line widths and spacings of $100\ \mu\text{m}$. Five signal conducting lines on one layer, and 5 other conductive signal lines on a layer beneath that, separated by an isolated layer. This way, the wiring to the outside world could be as narrow as $1.2\ \text{mm}$ (5 wires per layer, with a width of $100\ \mu\text{m}$, all separated by $100\ \mu\text{m}$, also on the exterior sides of the wiring part).

The entire design is of course coated by an isolating layer on all sides, except for the measuring spots. Since this creates some distance from the outer layer of the electrode to the measuring spot, it could be hard to establish good contact to the brain tissue. To bridge this gap, golden blobs were added to all the measuring spots by means of a wire bonding device. Not only did this resolve the issue of the gap between the outer layer and the brain tissue, it was also possible to make these blobs smaller in diameter (semispheres of a diameter of about $50\ \mu\text{m}$). A digital impression of the first design is given in Figure 5.2. The lower left corner shows a detailed view of the measuring tip. The triangular shape and the golden blobs are clearly visible in this impression.

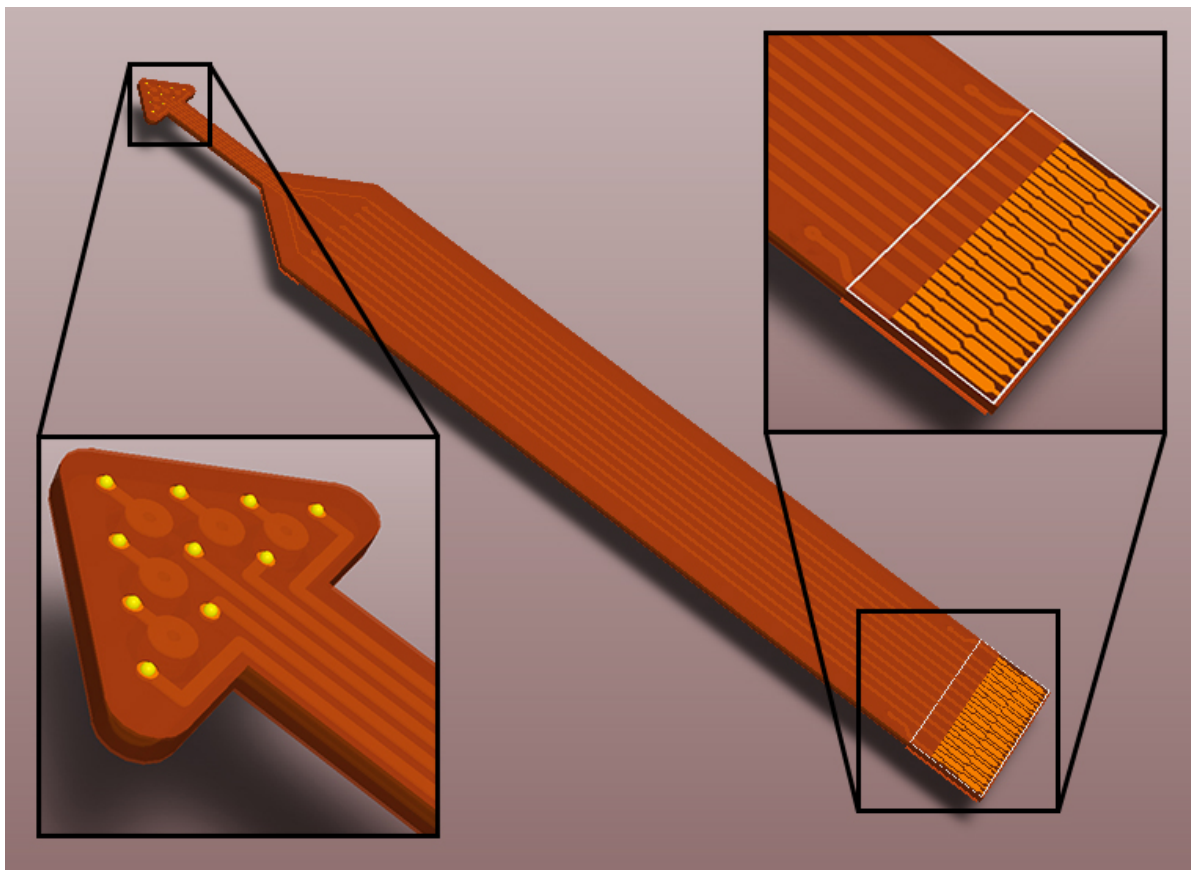


Figure 5.2: A digital impression of the electrode, tip and bottom are highlighted

At the other end of the electrode - the part opposite of the measuring side, outside of the animals body - a structure was created to act as the male side of a ZIF-connector (zero insertion force). The upper right corner of Figure 5.2 shows this part in detail. Another PCB was created to mount the receptor for this connection. Note that this type of connection allows for a total of 25 channels, of which only 12 were used in this design (10 measuring spots and two ground connections). This board was then used to mount wires with connectors compatible with the measuring setup in the lab. A similar digital impression of this board is given in Figure 5.3. Not only acted this PCB as a converter from PCB to compatible cables, it also allowed for quick replacement of the flexible electrode in case of failure or after a single use of an electrode (because of hygienic reasons).

To give an impression of the finished electrode, some pictures were taken of the complete design, the

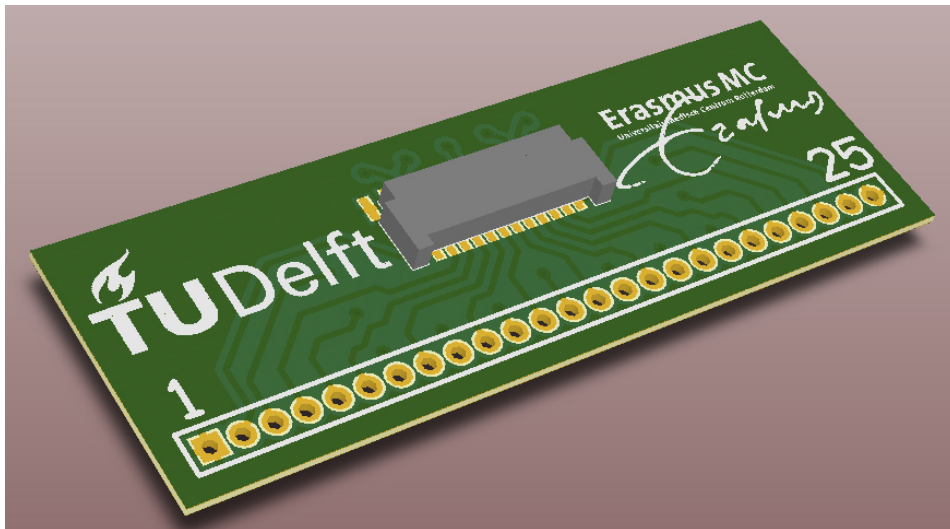
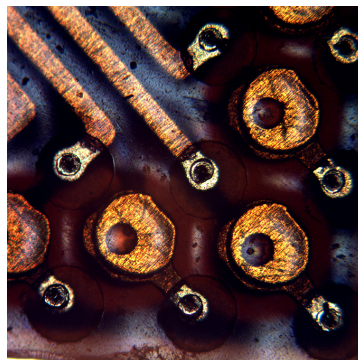


Figure 5.3: A digital impression of the receptor board

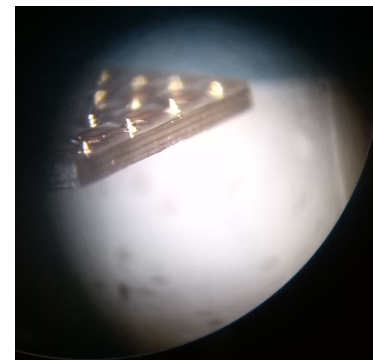
electrode tip and the added golden blobs. These can be found in Figure 5.4. The first image (Figure 5.4a) shows the total electrode design, including measuring tip at the top, and the connector at the bottom. The next Figure (5.4b) shows the measuring tip in detail. This picture was taken through a microscope. The large circles are the via's, connection the conducting layers to each other. The small dots are the measuring spots. Finally, Figure 5.4c shows a zoomed in image of the golden blobs at an angle, showing that these blobs extend from the surface, as they were supposed to. The complete system including the receptor board and wires with compatible connectors is show in Figure 5.5.



(a)



(b)



(c)

Figure 5.4: First electrode design, finished product

5.3. Characterization

Two parts of characterization were done on the newly produced electrode array. First of all, the array was tested in the measurement setup present in the laboratory in Rotterdam. This is described in Subsection 5.3.1. Furthermore, the impedance levels of the array are investigated in Subsection 5.3.2

5.3.1. Test signals

To test the newly designed electrode array, a testing session in the measuring laboratory in Rotterdam was done. Because the connections were chosen to be compatible with the current measurement setup, connecting the electrode array went very smoothly. To test the electrodes, multiple test signals were designed using Matlab. The electrode was hooked up to the system and the measuring tip was submerged in a saline solution. The test signals were transferred to the saline solution by means of a jack cable from a laptop audio output, which was altered to have a separate signal and ground wire at the

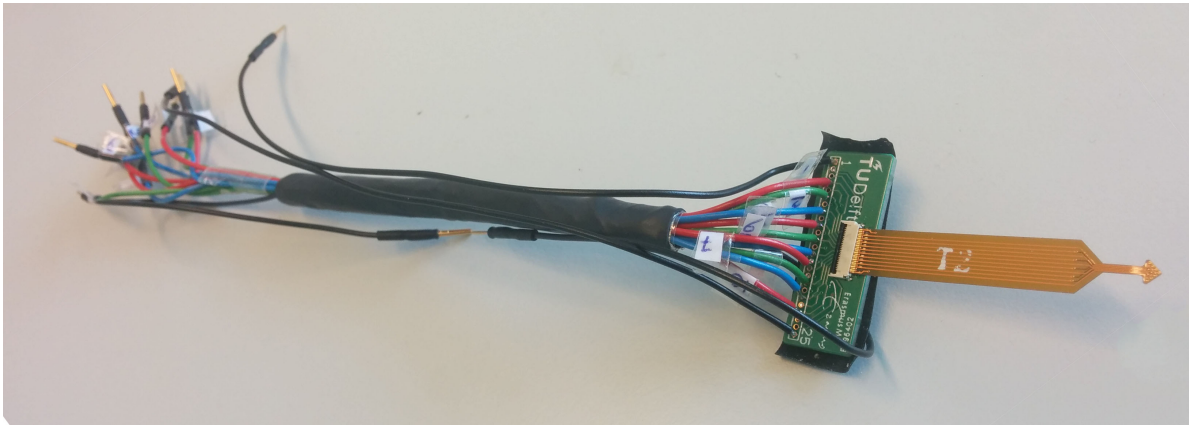


Figure 5.5: Overview of the complete system, including electrode, receptor board and cables

other end of the cable. The setup records the signal at a sampling frequency of 24414 Hz.

Since the measuring setup was designed for measuring brain signals, the test signals from the computer had to be attenuated to reach the same level of amplitude compared to brain signals. This was done using a simple resistive divider, although this does introduce some noise to the measurements. First of all, a variety of frequencies were created and applied to the saline solution via the jack-cable. Since the frequency range of the neural signals were presumed to be in the frequency range of 1 Hz up to 20 Hz. Secondly, a white noise signal was generated using Matlab and was applied to the saline solution. The result of one of these measurements is given in Figure 5.6. A frequency analysis of this recorded signal can be found in Figure 5.7. This specific data shows the recording of a 10 Hz signal applied to the saline solution. A few remarks can be made regarding this data.

- First of all, the 10 Hz signal can clearly be seen in the result, proving the connections to be working for the channels recorded.
- Second of all, there seems to be some interference from the mains at 50 Hz, since the peak at this location seems to be slightly higher than the previous harmonic at 30 Hz. This shows that the Faraday cage in which the experiments took place is not completely free of interference sources.
- The shape of the frequency analysis shows a low pass characteristic, which is as expected given the fact that the electrode array was submerged in a saline solution, which should give rise to a double layer impedance, as described in Section 3.1.

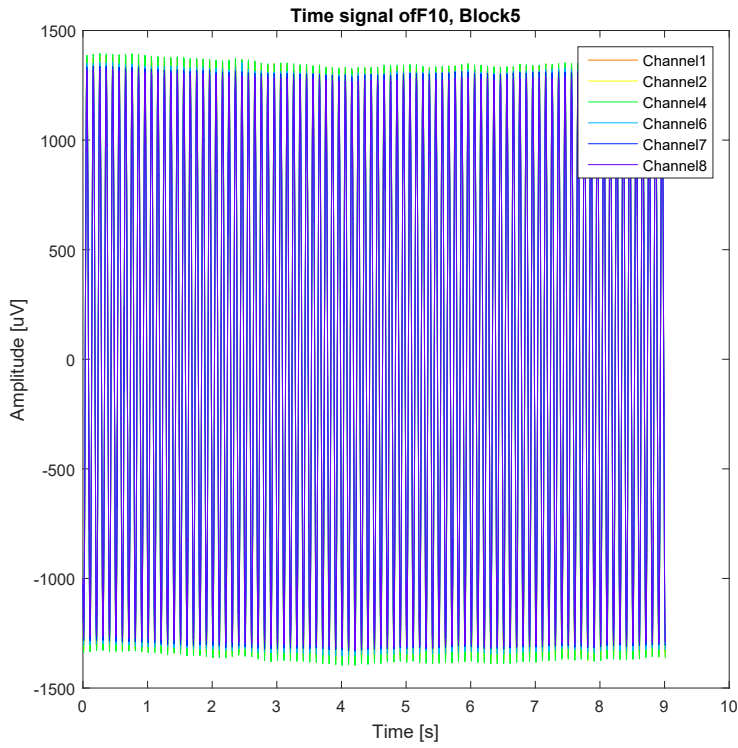


Figure 5.6: Time domain plot of measured test signals: 10Hz sinusoid

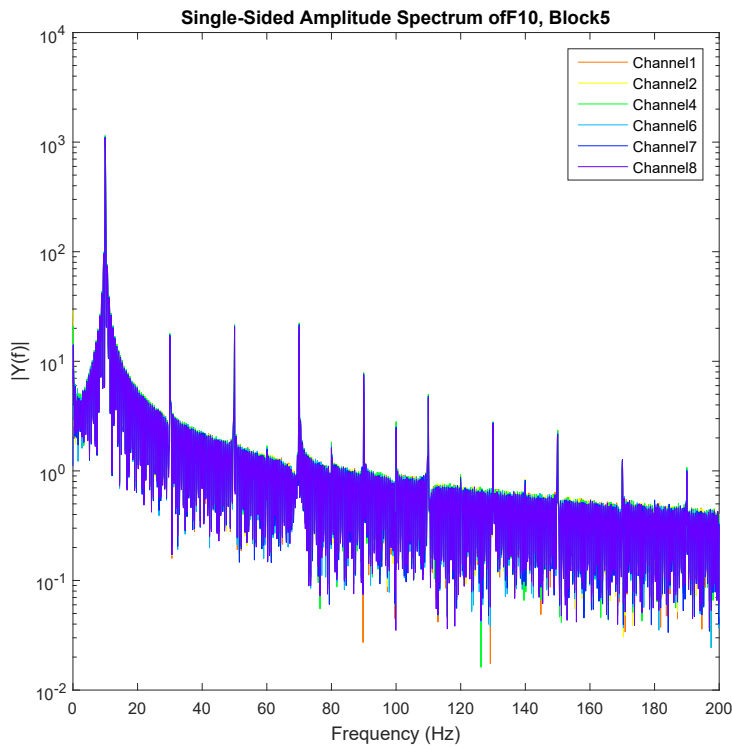


Figure 5.7: Frequency domain plot of measured test signals: 10Hz sinusoid

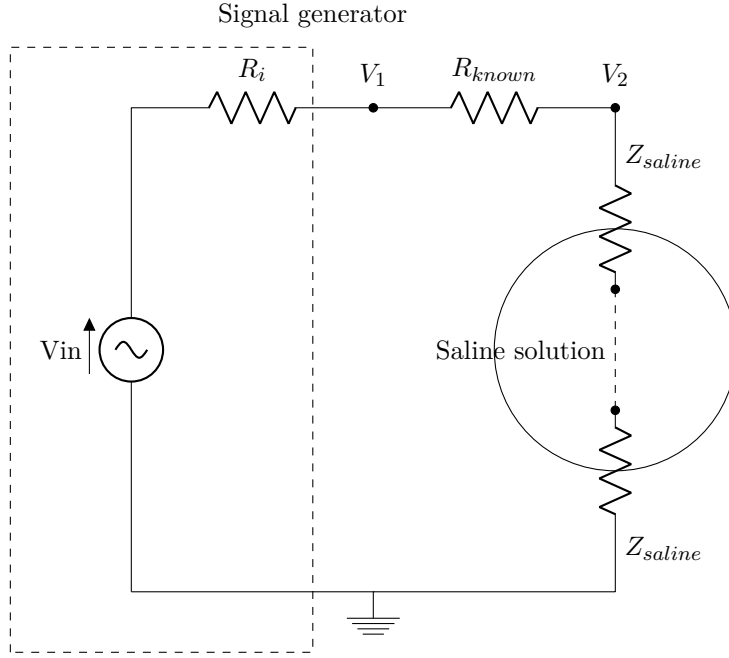


Figure 5.8: Measurement setup for analyzing saline double layer interface impedance

5.3.2. Impedance levels

To characterize the electrode array, a measurement was done to investigate the impedance levels. In order to apply a signal to the electrode array, the tip of the array needs to be submerged in conducting fluid. A phosphate buffered saline solution was chosen for this experiment. The fluid used consists of Sodium Chloride (90 g/L), Potassium Phosphate monobasic (1.44 g/L) and Sodium Phosphate dibasic (7.95 g/L) [19]. When a signal conducting wire is submerged in the solution, however, a double layer impedance arises (see Chapter 3), which influences the impedance measurement on the electrode array, so the first part of measuring the impedance of the array is to investigate the impedance of the interfaces between the cables and the saline solution. The setup for this first part is given in Figure 5.8.

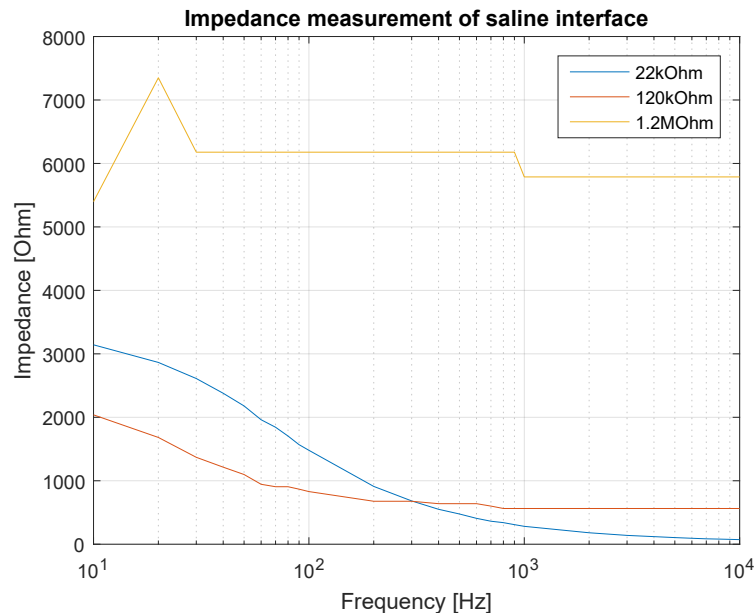
A signal generator (including V_{in} and an internal resistance R_i) is used to generate a sinusoidal voltage signal, which is applied to a known resistor in series with the unknown impedance of the saline interfaces. Note that two impedances are given in the figure: a metal wire leading the signal into the saline solution gives rise to a double layer impedance, the wire leading the signal from the solution to ground creates such an impedance as well. The voltage is measured across $R_{known} + 2 \cdot Z_{saline}$ (V_1) with respect to ground for a variety of frequencies. At the same time, the voltage across the two series impedances of the saline solution is measured with respect to ground (V_2). This way, the unknown impedance of the saline can be computed for each individual measured frequency as:

$$Z_{saline}(f) = \frac{1}{2} \cdot \frac{R_{known}}{\frac{V_1(f)}{V_2(f)} - 1} \quad (5.1)$$

Since the current is partly limited by the known resistor, and this current influences the charge time of the double layer capacitance, multiple resistor values and voltages were applied to see this influence. Table 5.2 shows the different setups used to analyze the influence of the resistor value. The results are shown in Figure 5.9. As expected, the interface between metal and the saline solution acts as a capacitor, but the influence of the known resistor is large. The lowest currents analyzed (125 nA) requires a very large resistor in combination with a very low input voltage. The voltage drop over the saline is therefore very low and very hard to measure. It is therefore very hard to really conclude anything about the saline interface from these measurements. The overall impedance does seem very low compared to the expected values of the impedance of the electrode array (6 k Ω versus 200 k Ω) (the metal wires are relatively very big compared to the measuring spots on the electrode). Therefore, the influence of the saline will be neglected in measuring the impedance of the electrode array.

Table 5.2: Applied voltages and resistors in impedance measurement

Known resistor	Voltage applied (peak-peak)	Maximum current
22 kΩ	5 V	227 μA
119 kΩ	150 mV	1.3 μA
1.2 MΩ	150 mV	125 nA

Figure 5.9: Impedance measurement of saline interface. Three values for R_{known} are used (22 kΩ, 120 kΩ and 1.2 MΩ).

To get to the impedance levels of the new electrode array (measured on only one channel), the metal wire connecting the saline solution to ground is now replaced by the electrode. Again, two voltages are measured, both across $R_{known} + Z_{saline} + Z_{electrode}$ (V_1) and across only $Z_{saline} + Z_{electrode}$ (V_2), both with respect to ground. The schematic for this measurement is given in Figure 5.11. Since the electrode impedance is now the only unknown variable, this impedance can be computed as given in Equation 5.2. Note that R_p appears in this Equation. This represents the resistance of the voltage probe used. Since this has a resistance of 1 MΩ, which is in the same order of magnitude as the expected impedance, it can not be neglected in this measurement.

$$Z_{electrode} = \frac{V_2 R_{known} R_{saline} + V_2 R_{known} R_{probe} + V_2 R_{probe} R_{saline} - V_2 R_{probe} R_{saline}}{V_1 R_{probe} - V_2 R_{known} - V_2 R_{probe}} \quad (5.2)$$

As described in Chapter 3, a simplified model of an electrode consists of three components: a spreading resistance (R_s), a double layer electrode resistance (R_e) and a double layer electrode capacitance (C_e). The data given in Figure 5.11 can be used to give an estimate of these values. At high frequencies, the impedance of the capacitance goes to zero, so the only component in the signal path is R_s . Different currents lead to a different measured values for R_s , but it will be in the order of a few tens of kilo-ohms (say 20 kΩ is a good estimation). At DC, the impedance of the capacitance goes to infinity, so the only remaining components in the signal path are R_s and R_e . The sum of these resistances can be estimated from the Figure to be around 200 kΩ. Since we estimate the spreading resistance to be around 20 kΩ, we can estimate the value of the double layer resistance at 180 kΩ. The value of the capacitance can be calculated by inspecting the cutoff frequency. In this case, the -3dB frequency is found at 50 Hz. Computing then results in $C = \frac{1}{2\pi f R}$ which leads to $C_e = 16$ nF. The values are summarized in Table 5.3. Calculating the impedance at 1 kHz (or reading it from the measurement) leads to a value of about 25 kΩ, which does meet the specifications.

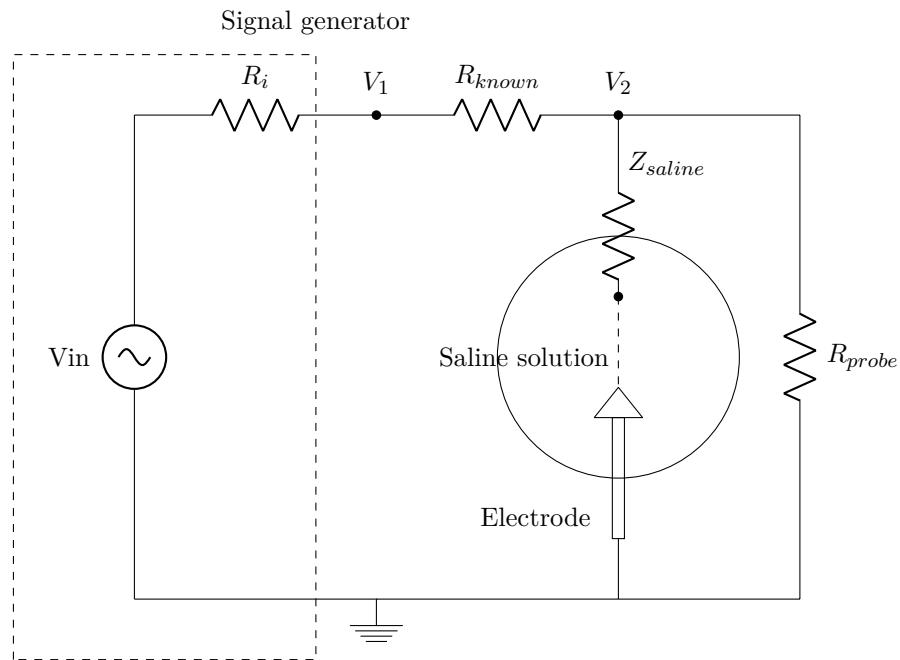


Figure 5.10: Measurement setup for analyzing the electrode impedance

Table 5.3: Impedance values for the electrode array, first design. $R_{known} = 1.2\text{ M}\Omega$ was used to come to these values, since the largest resistor limits the current to the most realistic value.

Component	Value
R_s	20 k Ω
R_e	180 k Ω
C_e	16 nF

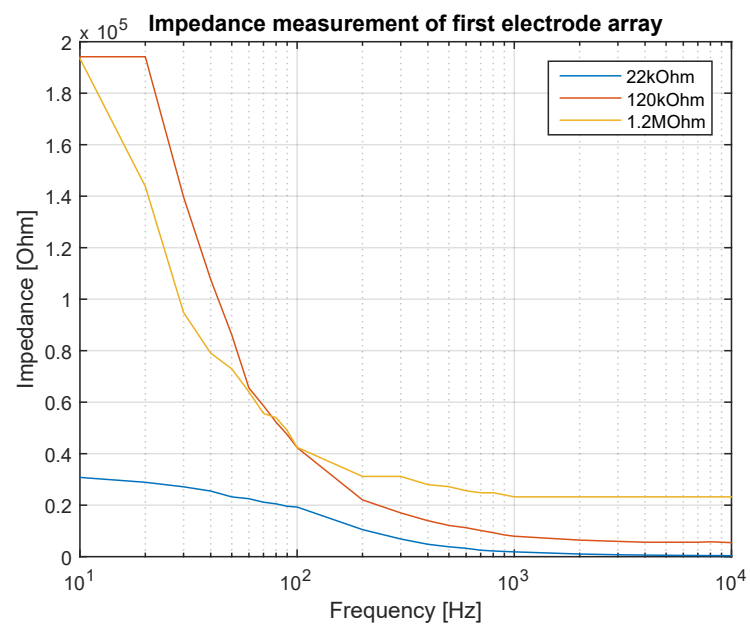


Figure 5.11: First design electrode impedance analysis

5.4. In vivo measurements

After the satisfying result of the dry run test measurements described in Section 5.3 the electrode design was used to carry out real in vivo measurements. The electrode design was hooked up to the measurement setup and was put in contact with the olivary tissue of a mouse. The setup is almost entirely placed inside a Faraday cage, to prevent distortion from signals outside of the cage (such as 50 Hz signals or radio waves). The only part leaving the cage is an optical fiber transferring measured signals from the measurement setup to a nearby computer for visualization and storage. A couple of measurements were performed. A part of one of these measurements is given in Figure 5.12. This Figure shows just two of the 10 available channels of the electrode array. A lot of signal quality variation can be observed between channels. Channel 12 and 13 are on the lower right part of the electrode, as viewed from the measuring side. These channels show the most promising signals, probably because the electrode array was not placed entirely flat on the surface of the olive creating a better connection for some channels than others.

To gain more insight in the information contained in this data, a frequency analysis is shown in Figure 5.13 and a zoomed in version (only 0 up to 25 Hz) in Figure 5.14. A few remarks can be made when observing these graphs.

- The signals from both channels are roughly showing the same signal, suggesting the they are both placed on the same tissue en recording the same structure. The fact the they are slightly different is a good sign, since signals in different locations of the olive should not be exactly the same but show a little phase shift.
- The zoomed out frequency analysis (Figure 5.13) shows a clear peak at 50 Hz and at its first harmonic at 100 Hz, although the measurement setup took place inside a Faraday cage.
- The zoomed in frequency analysis 5.14 further shows a peak slightly above 7 Hz, and also at the first and second harmonic 14 Hz and 21 Hz. This component is also clearly visible in the time domain as spikes every 140 ms. This signal probably correspondents to the electrical pulses associated with the heart beat, although this is a relatively high heart beat frequency for a mouse [20]. This might be explained by the fact that the mouse was relatively young and anesthetized [21].

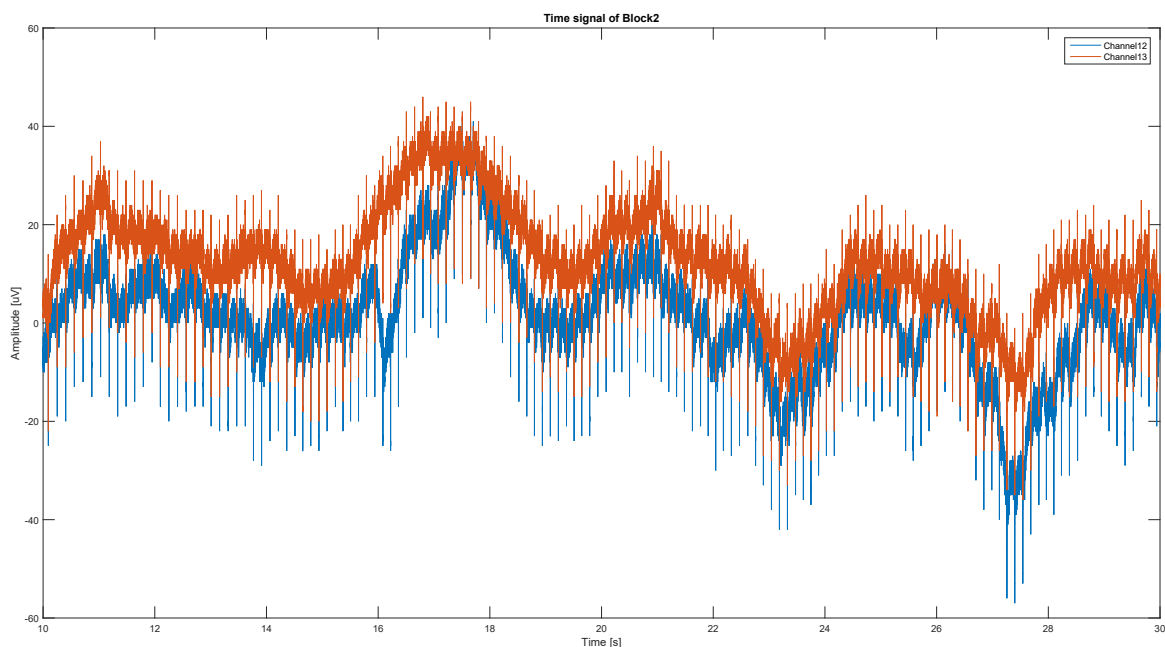


Figure 5.12: Part of an in vivo measurement using the first electrode design, time domain, 20 second measurement

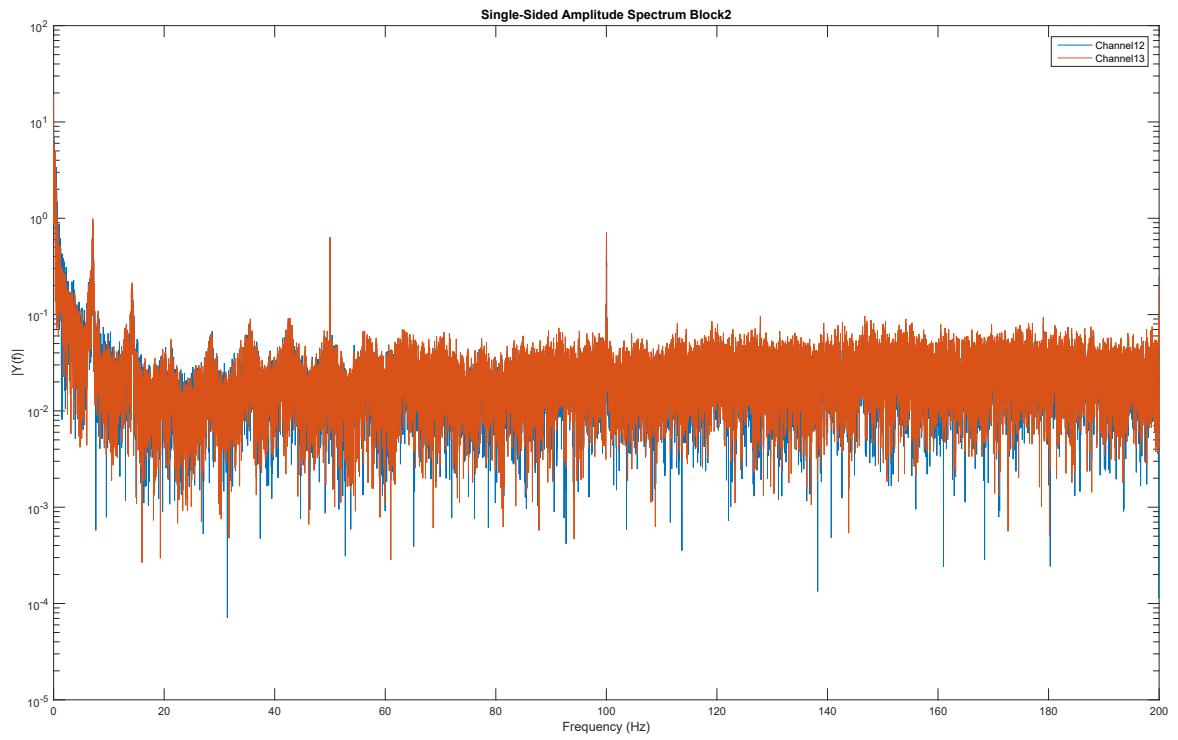


Figure 5.13: Frequency analysis of first in vivo data gained from first electrode design

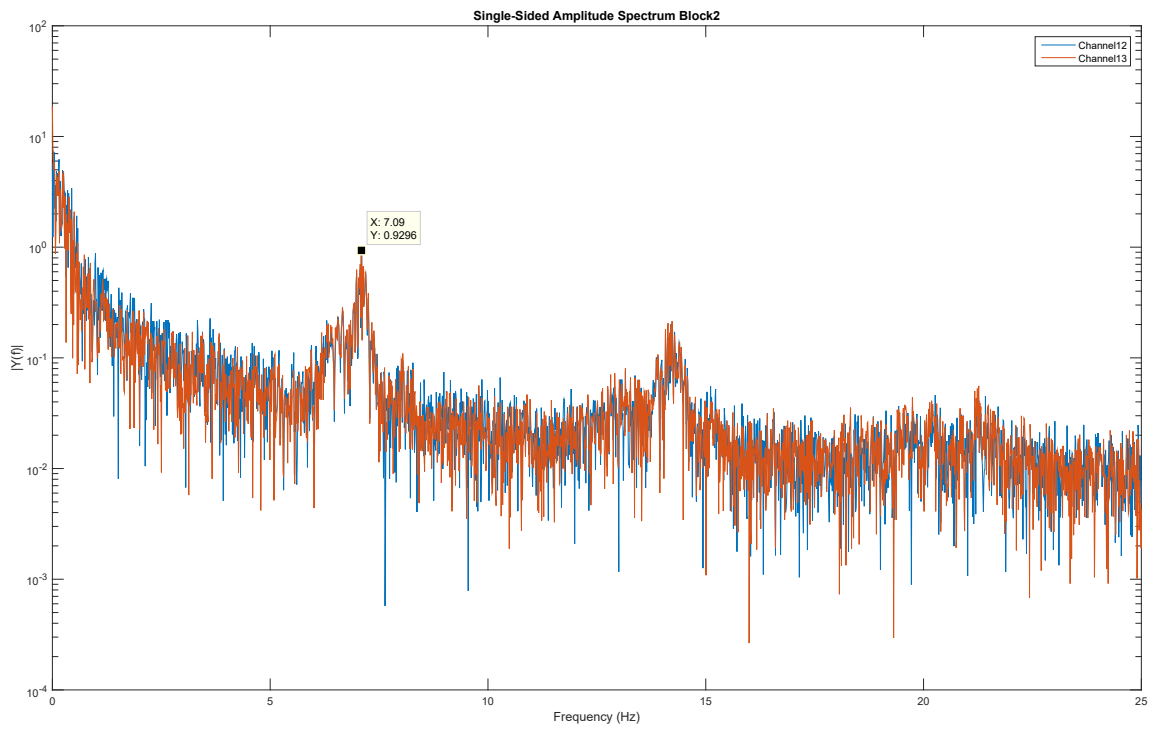


Figure 5.14: Zoomed in frequency analysis of in vivo data gained from first electrode design

5.5. Issues

Although the results from the first design seem promising, still some issues remain. Three issues were clearly observed in the first design:

- The golden blobs added on top of the measuring spots do not provide enough penetration into the tissue to ensure good contact with the tissue, especially since the measurements are ideally done outside of the dura to ensure long survivability of the animal. This is due to the fact that the structures are not that sharp and the golden material is relatively soft.
- The golden blobs are quite big, so the potential of multiple cells are measured at once. This way, timing differences between cells might be hard to observe since the average of a lot of cell is visualized with the measurement.
- The cables currently used are not sufficient. Not only are they too short and stiff for the surgeon to manoeuvre the device to the right location, they are also not shielded, which might cause the 50 Hz interference which was observed in the measurements.

These shortcomings in the first design needed to be overcome to do successful recordings. In order to accomplish a functional design, the electrodes used in the measurement setup in the laboratory in Rotterdam were investigated. This led to a second design, described in [Chapter 6](#).

6

Second electrode design: FlexPCB with tungsten tips

Reflecting on the shortcomings of the first design (Section 5.5), a new design was created, incorporating the electrodes used in the laboratory in Rotterdam and the first design electrode array described in Chapter 5. This chapter describes the design (Section 6.1) and characterization (Section 6.2) of this newly designed electrode. The results of in vivo measurements done with this electrode are described in Section 6.3. Finally, the issues that arose when using this electrode are addressed in Section 6.4.

6.1. Design

The Thomas Recording measurement array used in the laboratory used tungsten-quartz electrodes. This electrode starts off as a wire, and is heated in the middle of the wire. A pulling force then separates the wire into two parts. The part that was pulled forms a pencil-like structure, especially when polished further down with a specialized polishing machine. A schematic view of such an electrode is given in Figure 6.1, as the blue spike sticking out of the electrode design (cross section). These tungsten-quartz electrodes have a few benefits, which seem to overcome the problems that arose with the first design electrode: they are stiff enough to penetrate soft structures like tissue and they are small enough to be able to measure single cell size areas. The decision was made to incorporate these electrode tips on top of the triangular flexible design.

Since the scale on which we are working is very small, mounting the electrode tips on top of the surface electrode proved to be quite a challenge. First of all, the insulating layer was removed from two of the vias on the electrode to create conducting spots. The tungsten electrodes were then put through these holes to create a small needle of about 3 mm. With the use of pliers the quartz was removed from the tungsten core. This bare tungsten was then soldered on to the conducting layer of the surface electrode. To create stability, glue was added at the interface between the surface electrode and the newly added quartz electrode tips. Figure 6.1 shows the schematic overview of the created electrode. Figure 6.2 shows a photograph taken through a microscope of the finished product.

Besides the electrode, a few more minor modifications were done to the total setup. Since the 50 Hz interference was clearly observable in the first set of measurements, the regular cables were replaced by shielded cables (coaxial). Figure 6.3 shows the improved total setup. The shielding layers of the coaxial cables are connected to each other and a connector was installed to apply a signal to these shielding layers (ground, for example). The length of the cables was also increased, to improve the flexibility of applying the electrode to the brain of the animal.

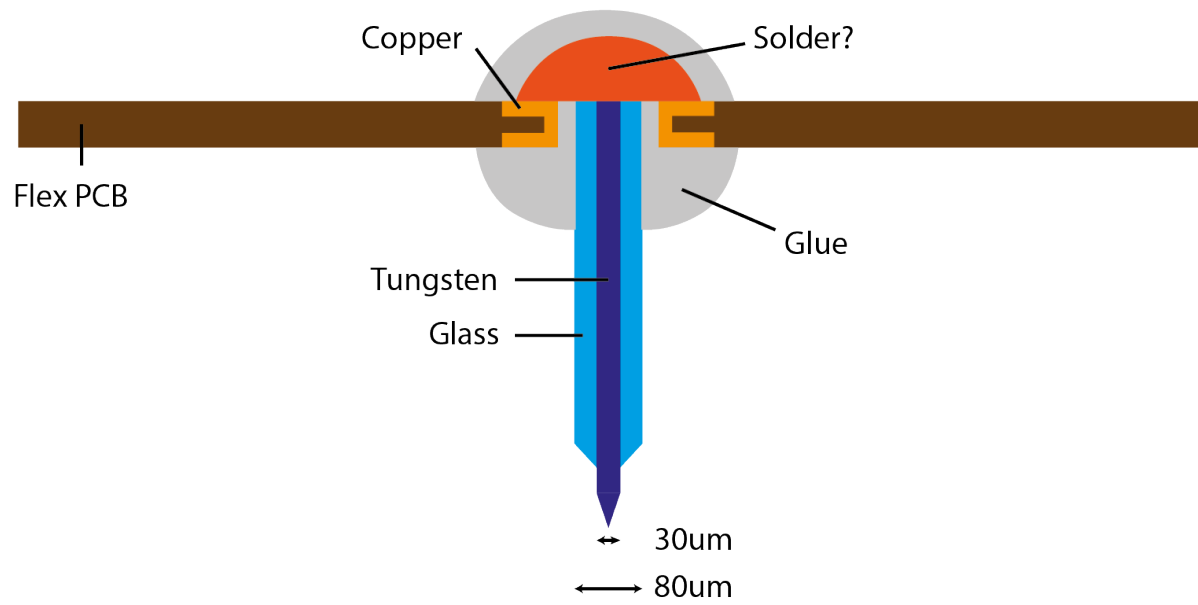


Figure 6.1: Schematic overview of the second design electrode, with tungsten tips

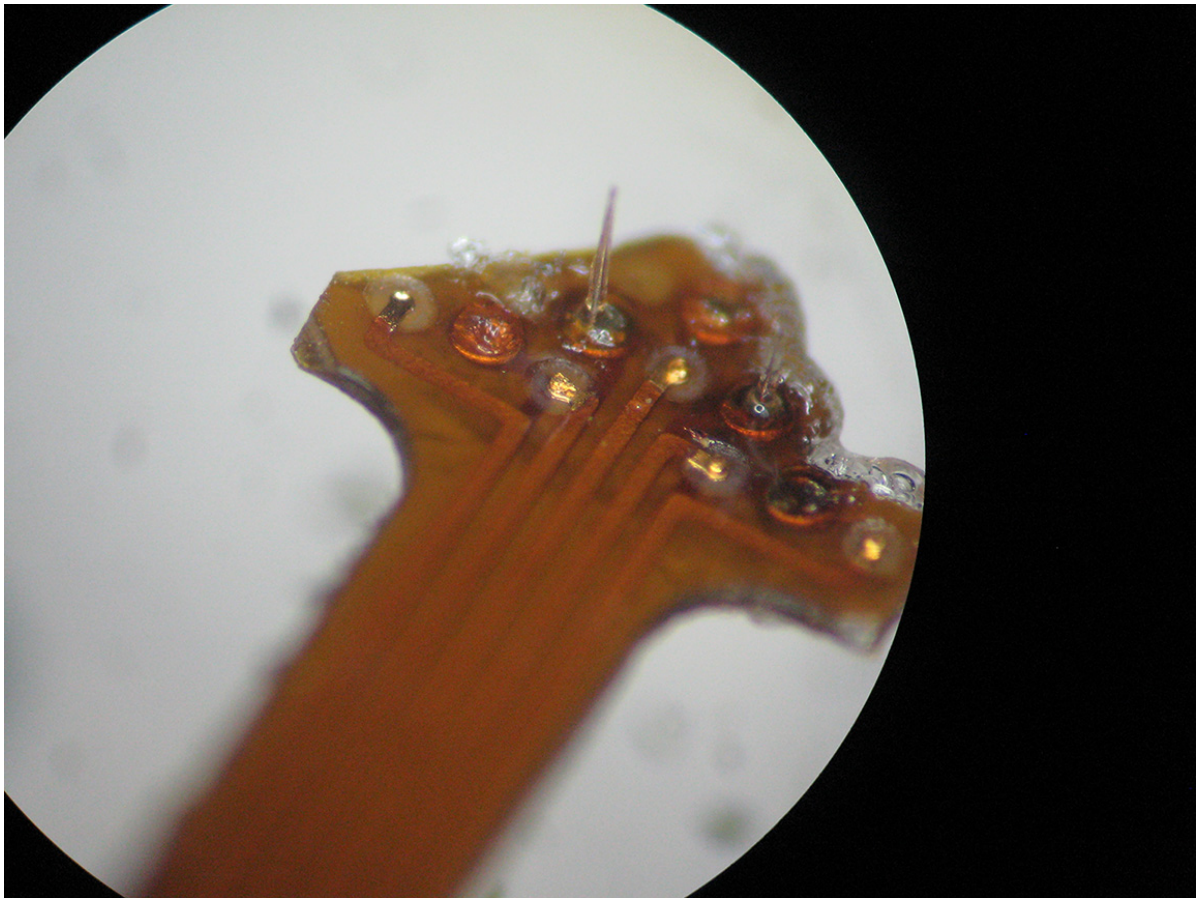


Figure 6.2: Photograph of second design electrode array with tungsten tips

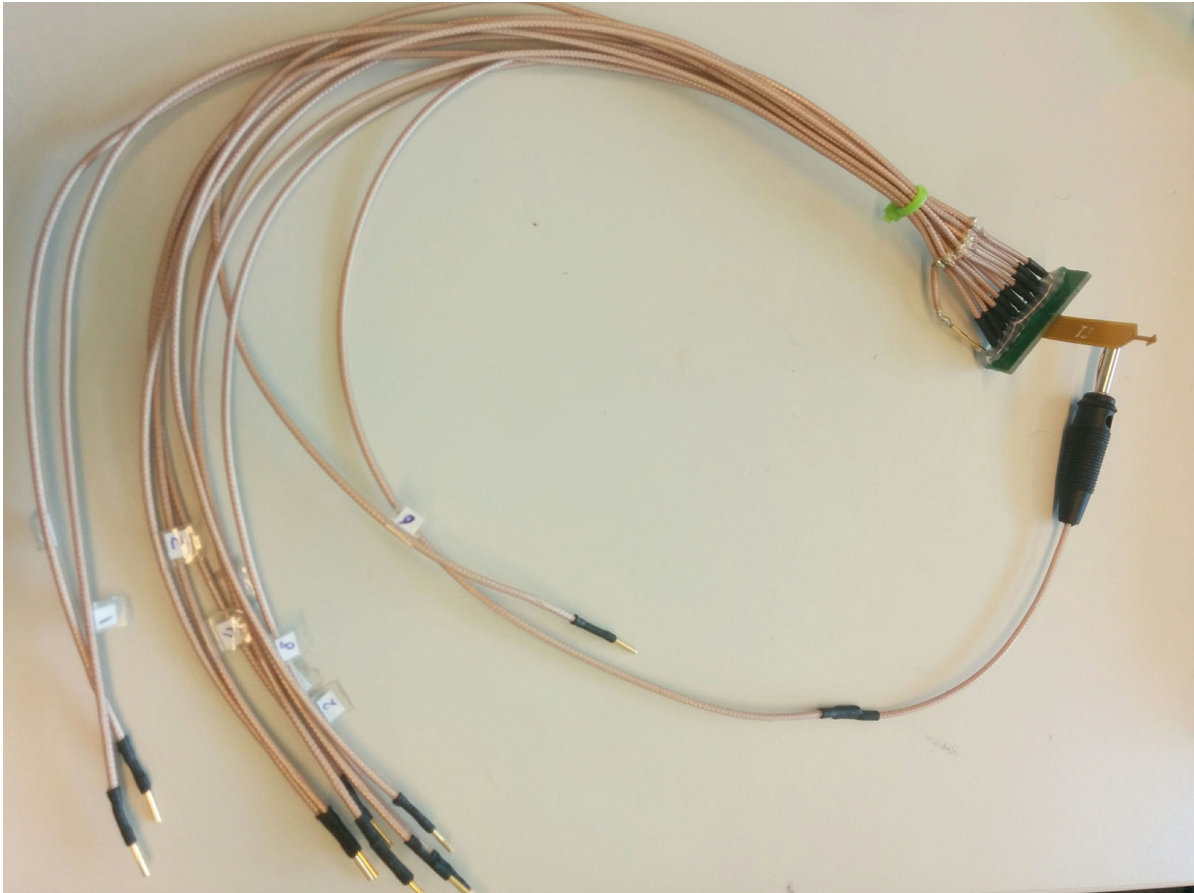


Figure 6.3: Complete setup with second design electrode array, mounted in the receptor board. Coaxial cables are installed to overcome issues with cable length and interference. The banana plug is installed to be compatible with the ground connection on the measurement setup, and can also be connected to the shielding layers of the coaxial cables.

6.2. Characterization

The major difference between the first design and this electrode array is the addition of the tungsten needles. These needles are placed on top of the existing electrode, and thus should change the impedance of the electrode. The same method as was explained in Subsection 5.3.2 was applied. The results were not satisfying. A decrease in current (caused by lowering the input voltage and increasing the known resistor value) led to a significant increase in computed impedance levels. Lowering the supply voltage and monitoring the impedances, it became clear that the impedance would rise way more when the current would be decreased more. Besides that, the specifications for such a grinded electrode (given in the order of mega-ohms) is measured with a current of only 5 nA, which is not reachable with this method at all, and therefore no comparison between the specifications of the grinded needle and this result can be made. This method was therefore abandoned. Instead, a Hewlett Packard 4194A was used to determine the electrode model component values. This led to the values given in Table 6.1. Note that these values may change when the tip of the tungsten needle is grinded differently (sharper or blunt, symmetrical or asymmetrical). Computing the impedance with these values at 1 kHz leads to an impedance of about 1.5 M Ω , which seems correct given the specifications of the electrode manufacturer. Worst case scenario, the impedance can go up even more. This specific needle, however, does meet the requirements set in Chapter 4, so grinding the other needles in the same way should be sufficient.

Table 6.1: Impedance values for a tungsten needle, found by the HP4194a spectrum analyser

Component	Value
R_s	20 k Ω
R_e	2 M Ω
C_e	100 pF

6.3. In vivo measurements

Since mainly the electrode of the system was adjusted, hooking up the electrode to the measuring system went exactly the same as with the first design electrode array. The longer cables proved to be a valuable addition to the system since the surgeon now has more freedom to apply the electrode tips to the brain tissue. The procedure of reaching for the brain structure was also not changed.

One thing that did change, however, was the addition of external stimuli to the animal. This was done by using air pressure. The air was guided to a tube and the tube was aimed at one of the whiskers of the mouse. The theory of the olive having a relation to rhythmic motor skills suggests that such a stimulus might lead to activation of this brain tissue and thus more interesting readouts.

6.3.1. Unfiltered data

A recording was done, including a brief period of air puff stimuli. The unfiltered data of this measurement is given in Figure 6.4. Already, the effect of the stimuli can be observed, although it is hard to see on this scale. Some artifacts can also be seen, especially around 100 s, when the measurement was shortly disturbed to adjust some cables. These artifacts can be ignored: only the periodic signals are valuable for the experiment. A zoomed in version, showing just a period of a few puffs is show in Figure 6.5. Here the reaction of the animal can be clearly seen. Since the electrical part of the stimulating device is located entirely outside of the Faraday cage and only a plastic tube guiding the air enters the cage, it can be concluded that the electrical activity can only come from the brain of the animal.

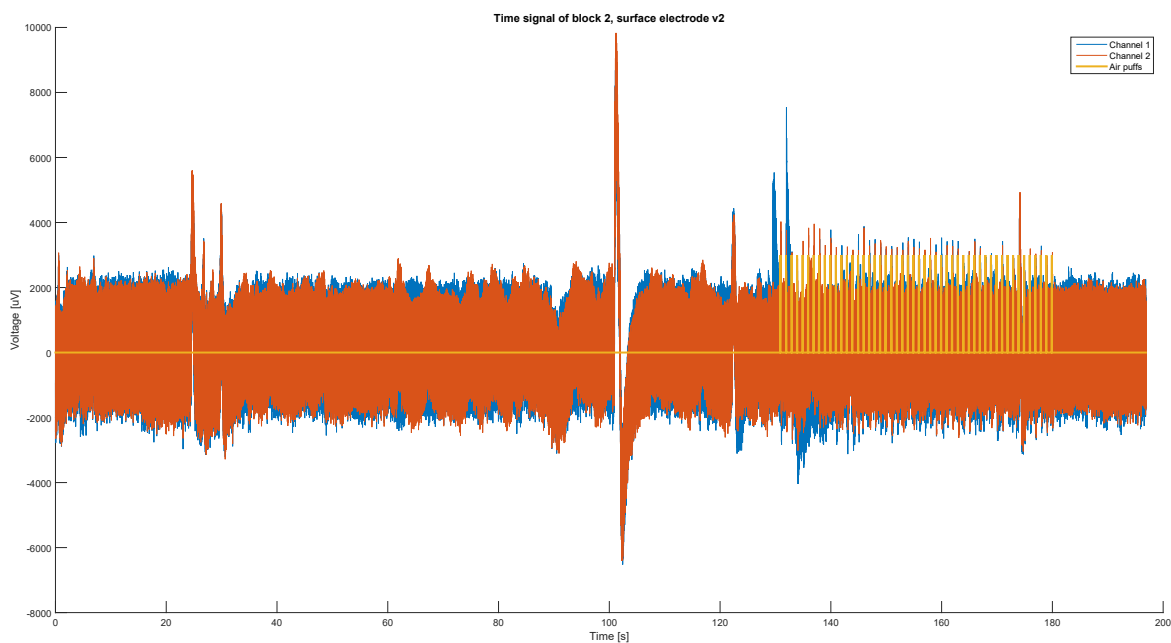


Figure 6.4: Unfiltered recording with the second electrode design

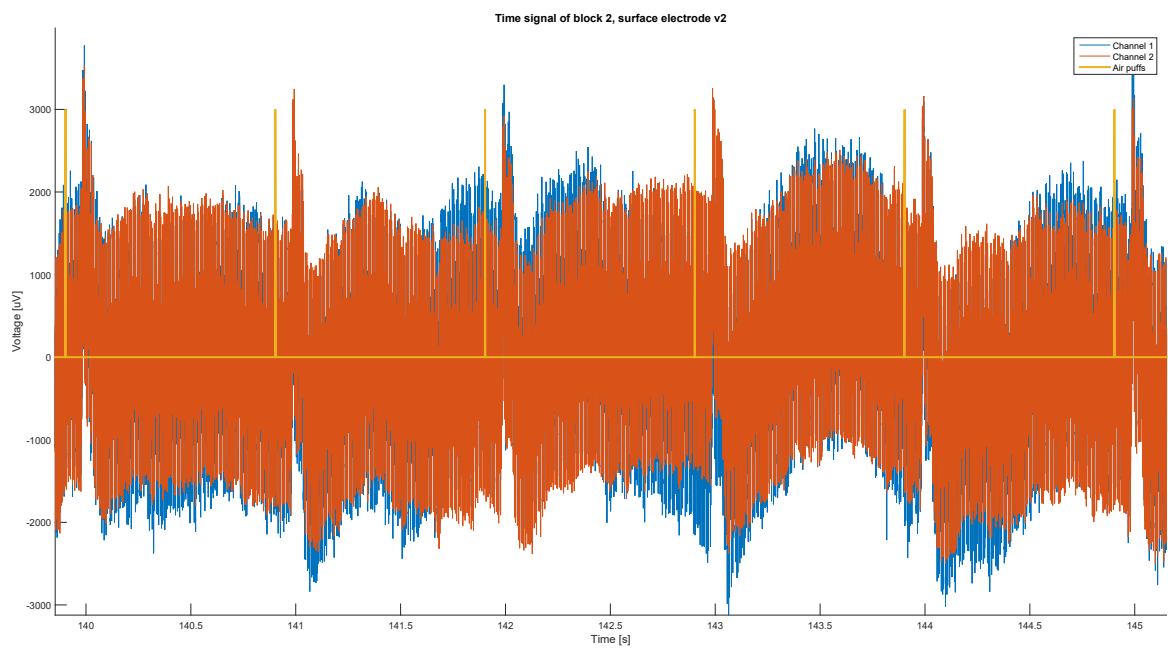


Figure 6.5: Zoomed in version of the unfiltered recording with the second electrode design

The signal is, however, still very rough and a lot of interference can still be seen. A frequency analysis was done to show the frequencies responsible for the interference. Figure 6.6 shows the frequency analysis for the range DC up to 2 kHz. Although hard to see clearly on this scale, a 50 Hz interference and its harmonics can already be observed (better visible in the zoomed in plots of this frequency analysis). Another point of interest in this spectrum lies at 450 Hz. No clear source for this interference has been found. Since the main region of interest is in the lower frequencies (say up to 200 Hz), a zoomed in plot of the frequency analysis is given in Figure 6.7 for frequencies up to 200 Hz and Figure 6.8 even further zoomed in for frequencies up to 50 Hz. From all these Figures, it can be clearly seen that the results would benefit greatly from filtering. The next subsection focuses on the processing done on the same signals.

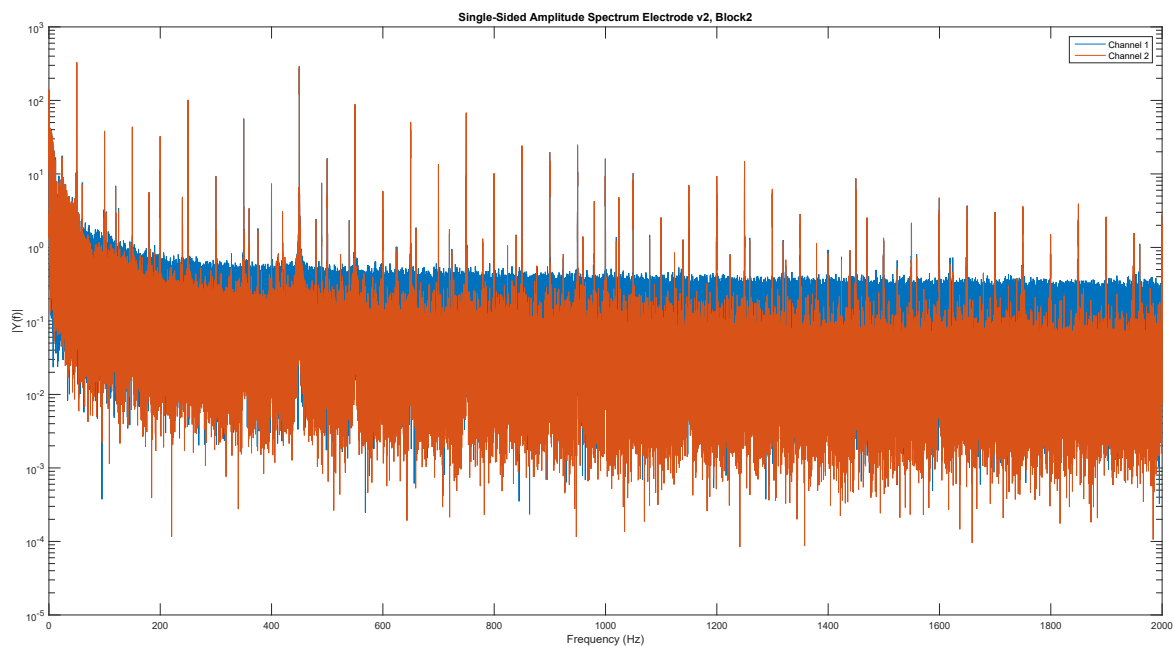


Figure 6.6: Frequency analysis of the measurement with the second electrode design including including air puffs, 0 - 2 kHz

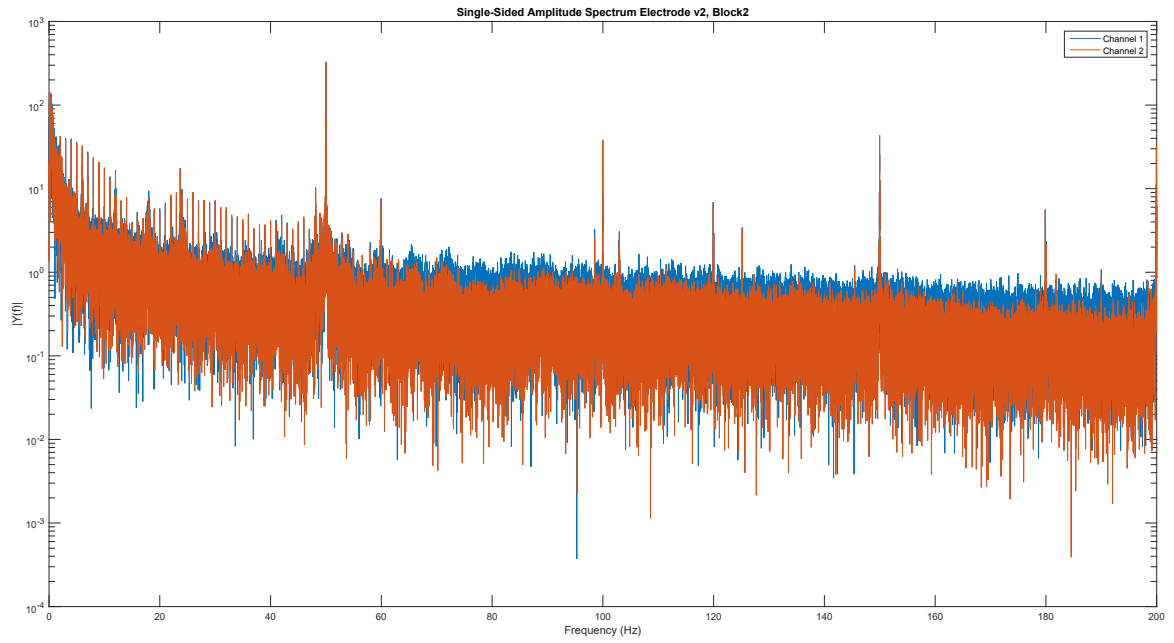


Figure 6.7: Zoomed in frequency analysis of the air puff measurement with the second electrode design, 0 - 200 Hz

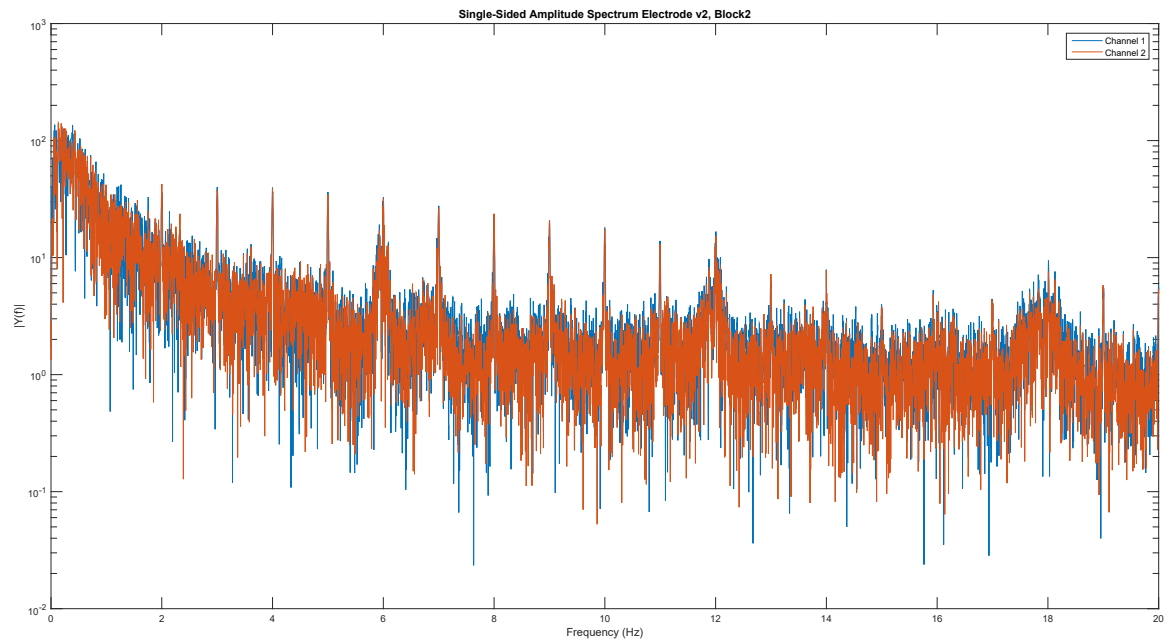


Figure 6.8: Zoomed in frequency analysis of the air puff measurement with the second electrode design, 0 - 20 Hz

6.3.2. Filtered data

To get rid of the unwanted influences presented in Subsection 6.3.1 multiple filters were designed and applied using Matlab. First of all, a comb filter was designed. A comb filter creates an interference with the signal itself by adding delayed versions of the signal to the signal itself. This leads to a response with a series of notches with a constant interval. These notches don't all have the same damping effect. When designing the filter, the first notch turned out to be only very mildly damping the signal (only about -0.25 dB), whereas the second notch damped the signal much more (-22 dB). It was therefore chosen to create intervals between notches of 25 Hz, creating the second notch at 50 Hz. For the rest of the notches, the same goes: the third notch is mildly damping, the fourth much more, creating the second big notch at 100 Hz, thus filtering the first harmonic of the 50 Hz distortion, and so on. Furthermore, a q-factor of 256 was chosen. The notches need to be very narrow, to ensure only the 50 Hz component is removed and no other frequencies in the signal, and therefore a high q-factor is needed. To create even more suppression, the filter was used twice in a row, creating even more damping at the frequencies of interference.

Now that the 50 Hz tone and its harmonics are suppressed, a low pass filter was designed to further increase the quality of the signal. Not only was the 450 Hz tone still present, but the signal does not contain much information in higher frequencies, so to reduce the noise this part can be filtered out. A low pass butterworth filter was designed with a cutoff frequency of 200 Hz. The filter was designed to be 6th order. This does however come at a cost. The main part of the brain waves we are interested in are below 200 Hz, but action potentials may also arise, which have components way higher than 200 Hz. This low pass filtering will decrease the speed of these spikes, making them lower and slower. Action potentials will still be roughly observable though, especially since the repolarization and after-hyperpolarization is not as fast.

The filtered data can be found in Figures 6.9 up to 6.12. First of all, all three frequency ranges as were presented in Subsection 6.3.1 are given. Figure 6.9 shows the comparison in frequency domain between the unfiltered and filtered signal. Only one channel is shown for each situation to be able to better observe the results. This Figure gives all frequencies up to 2 kHz. In this Figure, the low pass filtering can clearly be seen. At the cutoff frequency of 200 Hz the signal is attenuated about 2 times, which is as expected. The next plot (Figure 6.10) shows the same spectrum, but zoomed in to the range up to 200 Hz. In this situation, the effect of the comb filter, with clear damping at 50 Hz, 100 Hz and 150 Hz, can be observed. The third spectrum of this situation shows the range up to 20 Hz (Figure 6.11) Since the hypothesis presumes subthreshold oscillations in the range of only a few Hz (about 4 - 10 Hz [7]), it is vital for the data that these frequencies are left intact. The data shows an attenuation of signals up to about 1 Hz. Decreasing this value leads to less attenuation at the notches at 50 hertz and up since the notches get narrower (and since they don't have an infinite slope, the attenuation gets worse), so this situation was accepted to be sufficient. The data does show clear peaks at 1 Hz and all the harmonics above that, which could be caused by the stimuli given to the animal.

The real value of the filtering described before lies in the evaluation of the time domain data after the filtering is done. Figure 6.12 shows the time domain data after filtering. Only the moments with air puff stimulation are shown, since this turned out to be a region with interesting signals. An action potential of an olivary cell body is described in Section 2. The action potential observed in this measurement shows a delay of roughly 70 ms with respect to the stimulus. The action potential then shows an initial sharp peak (slightly slowed down by the low pass filtering), followed by a depolarization period of about 40 ms. After that a repolarization period of roughly 150 ms. This all seems consistent with the theory [7], suggesting correct recordings were done on the actual tissue of the olive.

This also leads to another clear and important conclusion: the olivary tissue seems at rest when no stimulus is applied. This seems to be consistent with the role of the olivary body, which is suggested to be involved in timing related motor functions, which are all shut down when anesthetized. The recordings done with the first electrode design were all without the presence of stimuli. Although the issues with this design needed to be looked into anyway, it can not really be concluded whether this design leads to correct measurements, since we only looked at the tissue at rest.

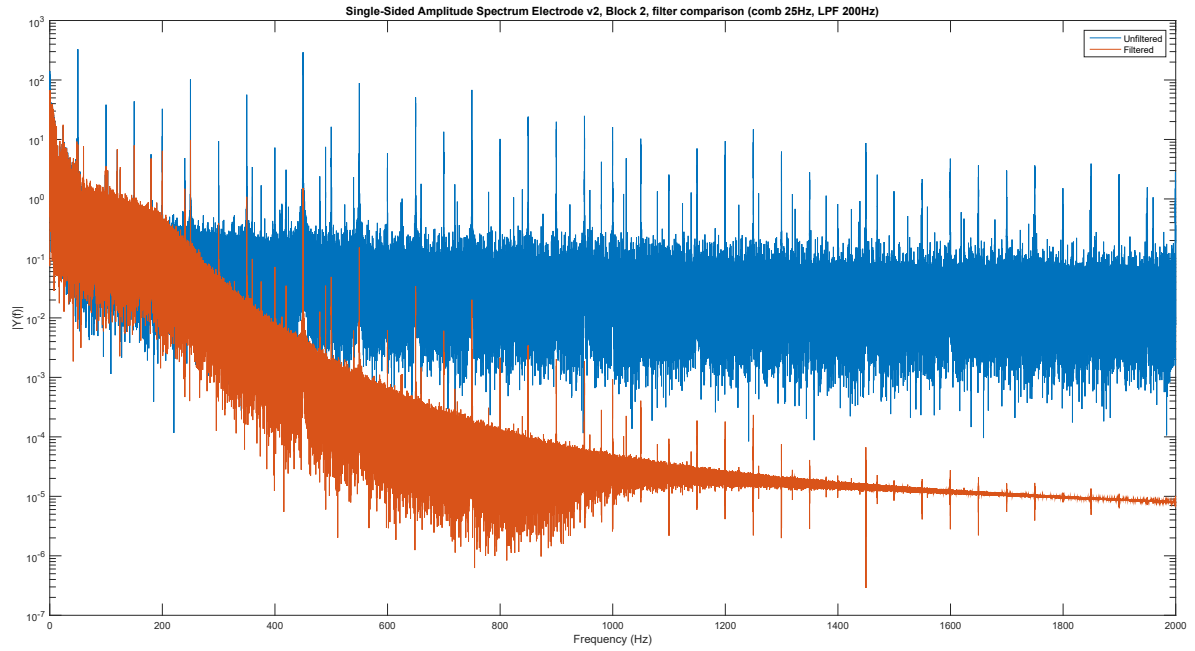


Figure 6.9: Frequency analysis comparison before and after filtering, measurement with the second electrode design, 0 - 2 kHz

One thing that is however not observable in the measurement is the propagation of the signal from channel to channel. This might be due to the sampling frequency used by the measurement setup of 24414 Hz. Since the measuring spots on the electrode are only about $500\ \mu\text{m}$ apart, the maximum observable propagation speed that is about $6\ \text{m/s}$, which is relatively slow since neural conduction speed can go up to $15\ \text{m/s}$ for the myelinated (B-) fibers that are present in the motor neuron system [4]. Action potentials can travel directly through the gap junctions present in the olivary system, so in this case the propagation might be even faster.

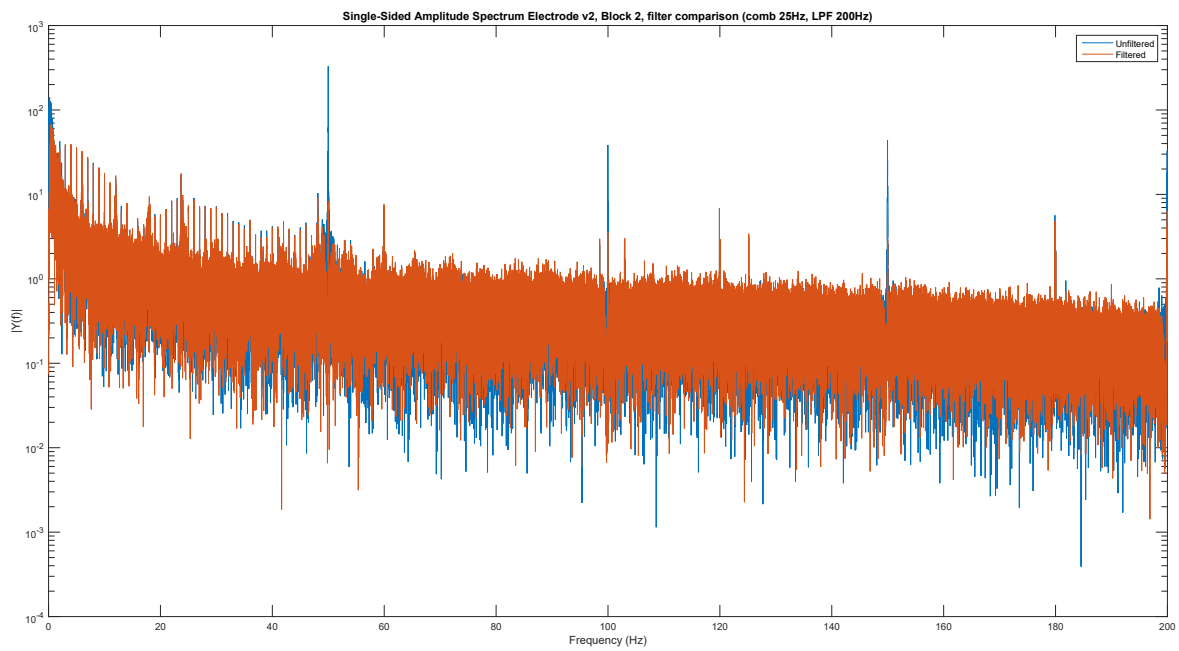


Figure 6.10: Zoomed in frequency analysis comparison before and after filtering, measurement with the second electrode design, 0 - 200 Hz

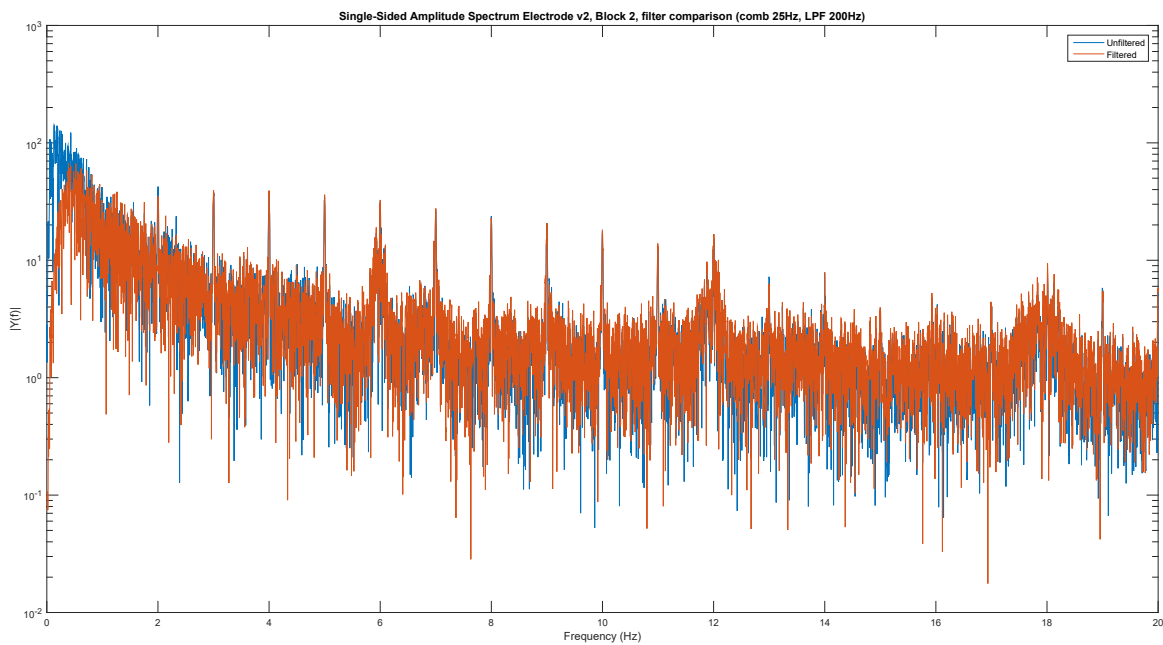


Figure 6.11: Further zoomed in frequency analysis comparison before and after filtering, measurement with the second electrode design. 0 - 20 Hz

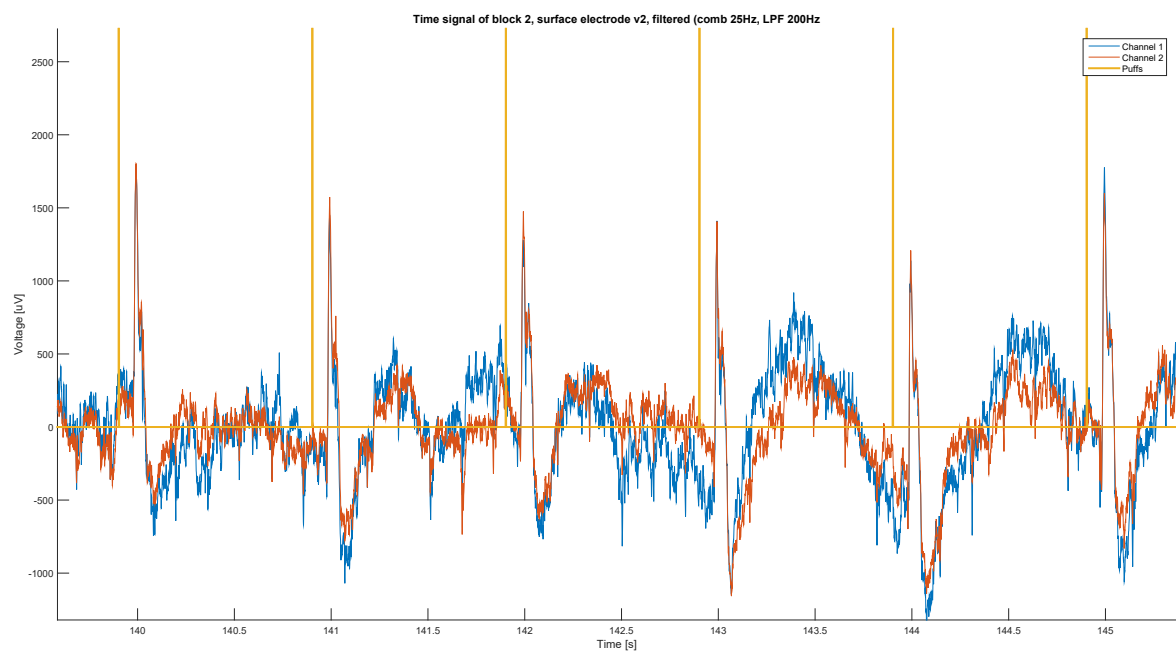


Figure 6.12: Filtered time domain data, zoomed in to part with stimuli, second electrode design

6.4. Issues

Although good results have been achieved, a few issues remain with this second electrode design, which are listed below.

- The small tungsten quartz needles perform excellent when looking at their penetrative power and area size, but they are very fragile. When putting a longitudinal force on the needle, they can handle a lot of force. A transversal force however causes the needle to break from the structure. One can handle the electrode design with great care and thus keeping the structure intact when applying it to the brain of the animal, but the animal itself can also move. The head of the animal is fixated during the measurement procedure, but still cardiac and respiratory movements can cause the structure to break.
- The procedure of applying the tungsten needles to the FlexPCB is very hard. During the procedure, the chance of breaking a needle is very likely to happen, and the process needs to be started over. Besides that, since everything was done by hand, the actual length of the needle can vary quite a lot, making the electrode hard to reliably reproduce.
- Although every measurement was done inside of a shielding cage and using shielded cables, some interfering signals can still be clearly observed. In order to avoid heavy post processing in future experiments, the structure needs to be evaluated, as well as the measurement setup itself. External sources surrounding the Faraday cage might be the cause of the 50 Hz signal still being clearly present, so these influences need to be eliminated.

Since measurements have been done successfully, the main focus now lies on creating a robust structure, which should ensure reproducibility and stability during measurements. To do so, another production technique was explored: 3D printing. The next chapter elaborates on the third design electrode array using this technique.

7

Third electrode design: 3D printed

To overcome the issues that arose when using the second electrode array design, a different approach was chosen. The previous models were flat structures with the measuring spots on the side, so they had to be bended in order to reach the tissue of the inferior olive. Since the structure of the electrode is quite fragile, this procedure is not desirable. This Chapter describes the new approach, which went through a few iterations to obtain the final design.

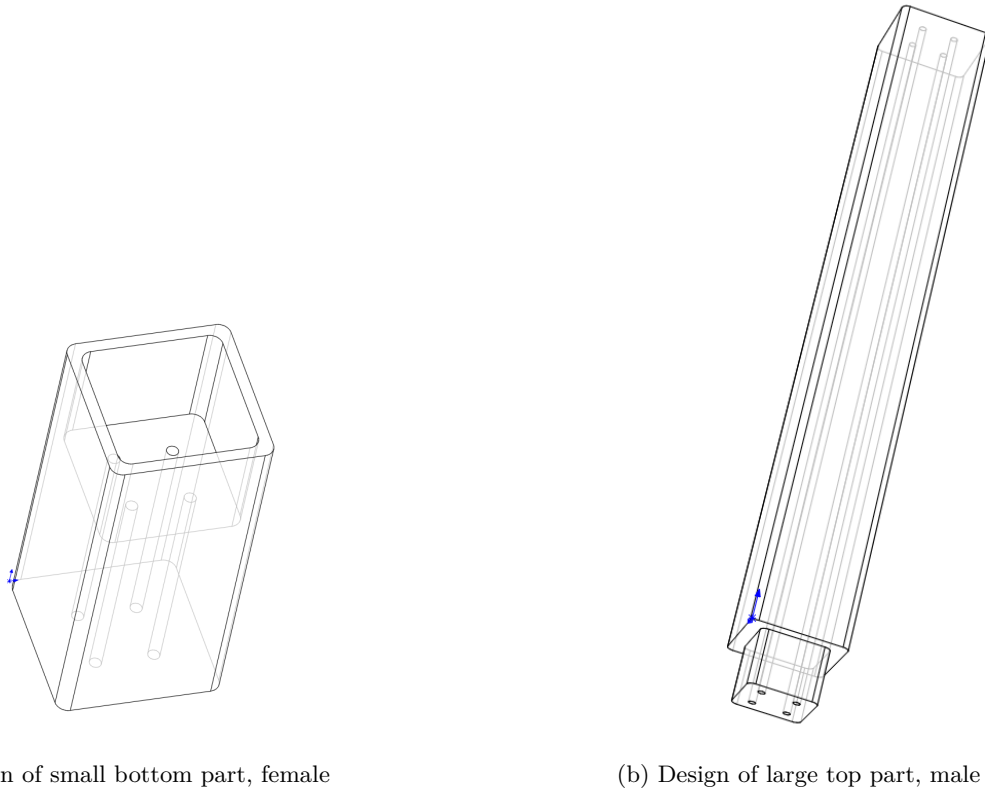
7.1. First design

During measurements, the previous approach of a flat structure which needed to be bended turned out to be quite a challenge to work with. First of all, the applied tungsten-quartz needles are very fragile, so they can easily break during this process. Second of all, since the main material of the electrode is flexible (FlexPCB), not a lot of force can be applied to the electrode to ensure good positioning.

The idea arose to create a straw-like structure. Inside this straw, the tungsten needles are applied and fixated, and this way no bending of the electrode is required since the needles are already in the longitudinal direction of the electrode design. When using this simple method, however, a few aspects of the electrode are very hard to control, mostly the spacing of the measuring tips. Therefore, the decision was made to use 3D printing technology to create the desired structure for the electrode, and then apply the tungsten-quartz needles to this structure.

The principle of the first design was as given in Figure 7.1. The design consists of two parts: a small bottom part (Figure 7.1b) and a long top part (Figure 7.1a). Both parts have 4 holes with a diameter of $100\ \mu\text{m}$. The two parts are to be clicked together like lego-blocks, and glue can be applied in between the two parts to fixate not only the two parts of the electrode but also the tungsten needles inside. The width of the structures is chosen to be $1400\ \mu\text{m}$, to ensure the objects are small enough to reach the targeted brain tissue. The height of the small bottom part was chosen to be $3\ \text{mm}$, the height of the large top part $10\ \text{mm}$, although these values are arbitrarily chosen and could be adjusted to meet the needs of the surrounding measurement setup. At this stage, no clear plan was made as to how to connect the tungsten wires to the readout system.

This design was printed using a Stratasys Objet350 Connex3, available for use at the faculty of Industrial Design Engineering of the Delft University of Technology. This machine is supposed to be accurate enough to create structures with features of $100\ \mu\text{m}$, since it promises a resolution of down to $16\ \mu\text{m}$ and an accuracy of down to $20\ \mu\text{m}$ [22]. Pictures of the result are given in Figure 7.2. A few remarks can be made by simply looking at the printed models. First of all, no hard lines can be seen: all the edges are smooth, therefore not creating the lego-like structure. Secondly, the walls creating the hole of the lego structure of the bottom part are much thicker than designed (difference between Figure 7.1a and 7.2a). Third of all, not visible in the images shown, the $100\ \mu\text{m}$ holes are not present at all. Clearly the scale of the models proves to be an issue in working with this technique. Since the printer manufacturer promises a high enough resolution for such structures, the decision was made to characterize the printer



(a) Design of small bottom part, female

(b) Design of large top part, male

Figure 7.1: Overview of the first 3d-printed electrode design

and create a second electrode design based on the findings in this process.

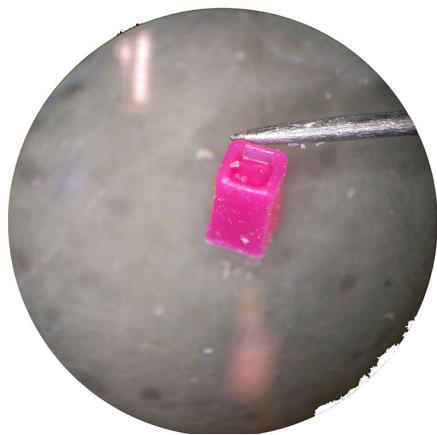
7.2. Printer characterization

To characterize the 3D printer, a model was made with all relevant structures. this model is described and shown in Subsection 7.2.1. During this process, the cleaning of the models turned out to be an issue at this scale, so some further tests were done to optimize this cleaning method. This is described in Subsection 7.2.2. The last Subsection (7.2.3) gives the results of the minimal sizes after cleaning the model.

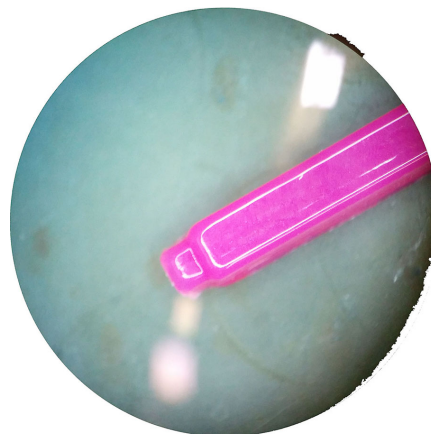
7.2.1. Dimension tester

A model was created to test multiple aspects of the 3D printer used. The design is shown in Figure 7.3. For the 3D printed electrode, a few aspects are relevant to investigate: minimal hole size, both horizontally and vertically, minimal wall thickness and minimum slit size. The model offers a variety of all these aspects, varying from very small (very likely too small) to relatively big. Since the printer builds the model layer by layer from the ground up, it might be relevant to investigate both horizontal holes and vertical holes, since they are created in a different way. Besides that, the length of the vertical hole is varied to see whether a hole in a thin part of the model could be lower in diameter than a hole in a thick part of the model. The tested dimensions are as follows:

- Vertical hole sizes: 100 μm , 200 μm , 300 μm , 400 μm , 500 μm and 1000 μm
- Height of vertical holes: 1 mm, 2 mm, 5 mm, 10 mm,
- Horizontal hole sizes: 100 μm , 200 μm , 300 μm , 400 μm , 500 μm and 1000 μm
- Standing wall thickness: 100 μm , 200 μm , 500 μm and 1000 μm
- Slit widths: 200 μm , 500 μm and 800 μm



(a) Printed small bottom part



(b) Printed large top part

Figure 7.2: Overview of the first 3D printed electrode

7.2.2. Cleaning process

The type of 3D printer used uses a fluid to create the model. A small droplet is applied at the right position in the layer and is shortly exposed to UV-light in order to solidify the material. To ensure good placement of the droplet, support material is printed in areas where no 3D printed material needs to go, so surrounding the model, in holes and underneath overhanging structures. This support material is a softer type of plastic which can be removed by hand from the model. To ensure better cleaning, high pressure water jets are often used to clean models. In this case, however, both these methods (mechanical hand cleaning and water jets) are not suited for cleaning, since parts of the models are just too vulnerable for large forces.

Another possibility is cleaning the models using chemical treatment. The manufacturer suggests lye (sodium hydroxide, NaOH) as a good dissolvent for the support material. It might, however, also affect the main building material of the model. To test the process, multiple test models (waste models including support material) were treated with different concentrations of NaOH for different periods of time. Models were submerged in a 2% solution, a 5% solution and a 10% solution, for periods of 15 minutes, 1 hour and 12 hours.

The main material of the 3D models turned out to be not visibly affected by the chemical treatment for the solution of 2% and 5%. The edges seemed a bit rounded off however in the case of long exposure to the 10% solution. The support materials did soften up or disappear after long enough exposure to the NaOH. A better effect was observed with higher concentrations of NaOH. The same goes for the period of time: as can be expected, more material was dissolved after a longer exposure time.

These results lead to a chemical cleaning process with a solution of 5% sodium hydroxide for a longer time. Most models were applied to the solution overnight, so for a period of 12 to 16 hours, with good results. Especially longer holes seem to benefit from longer exposure times, since the dissolvent only works on the surface of the support material, and thus needs time to reach the material in deeper parts. After the exposure, the models were thoroughly cleaned with water, not only to remove any leftover support material, but also to ensure safe handling of the model.

7.2.3. Results

The model described in Subsection 7.2.1 was cleaned using the process described in Subsection 7.2.2. An image of the finished product is shown in Figure 7.4. Photographs were taken of the finished model. The resulting dimensions were subsequently determined using ImageJ software, calibrated by means of a ruler in the same photographs as the model. Although this does not guarantee a micrometer precision measurement, it does give enough information to be able to adjust the electrode model to a stable design.

The weak walls have already collapsed because of the cleaning process. The narrowest wall did not

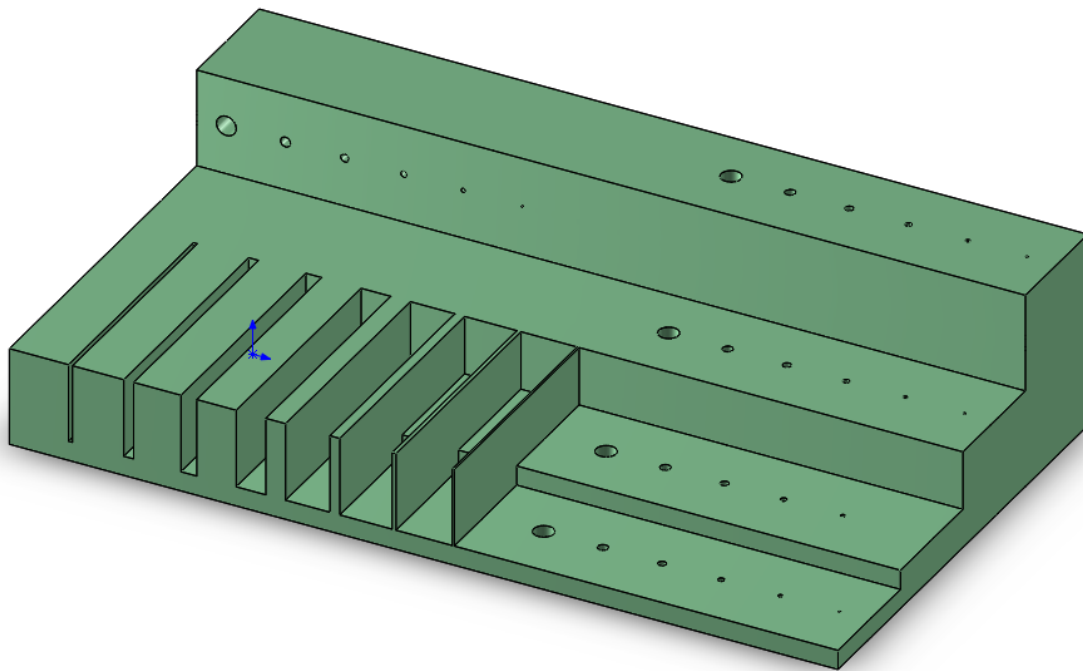


Figure 7.3: Design of the model to characterize the 3D printer

even have main building materials present. Only the wall of width 1 mm seems to be a stable result. Since the walls of the lego piece in the first design was only 200 μm wide, the design needs to be adjusted quite drastically to meet these specifications.

The slits all seem stable and the width was measured to be just as designed. Only the smallest slit (200 μm) is a little wider than designed (about 260 μm), but this is mainly due to the cleaning process, since the softened support material was removed by means of sliding a cardboard card between the slit.

The horizontal holes are all visible and opened up, except for the smallest hole (100 μm). Most of the holes are somewhat bigger than designed (for example: the 300 μm hole was measured to be about 330 μm), also due to the removal of the inner softened support material by means of a needle.

The vertical holes are the most troublesome in this model. Since the printer technique uses a liquid as its building material, small diameter holes are easily narrowed because of the fluid spreading before solidifying. This effect seems stronger when the hole is higher: the 1 mm high platform shows visible and clear holes as low as 200 μm , whereas the 10 mm platform only shows clear and open holes from 500 μm and bigger. The current electrode design was made of a solid body with holes throughout, so comparable to this high platform test model. With this knowledge, it is no surprise that the intended 100 μm holes were not visible in the previous design.

7.3. Second design

The results of the printer characterization described in Section 7.2 forms guidelines for an improved 3D printed electrode design. One of the clear observations was that small hole diameters can only be achieved when the height of the holes is relatively small. Therefore, a hollow design was chosen. This lead however to an issue: all hollow parts need to be cleaned from support material, as mentioned in Subsection 7.2.2. To overcome this issue, the design was broken into two parts: a small hollow part which is going to contain the tungsten-quartz needles and a larger top part which contains regular cables which are compatible with the readout system. Since the two parts need to be able to be connected

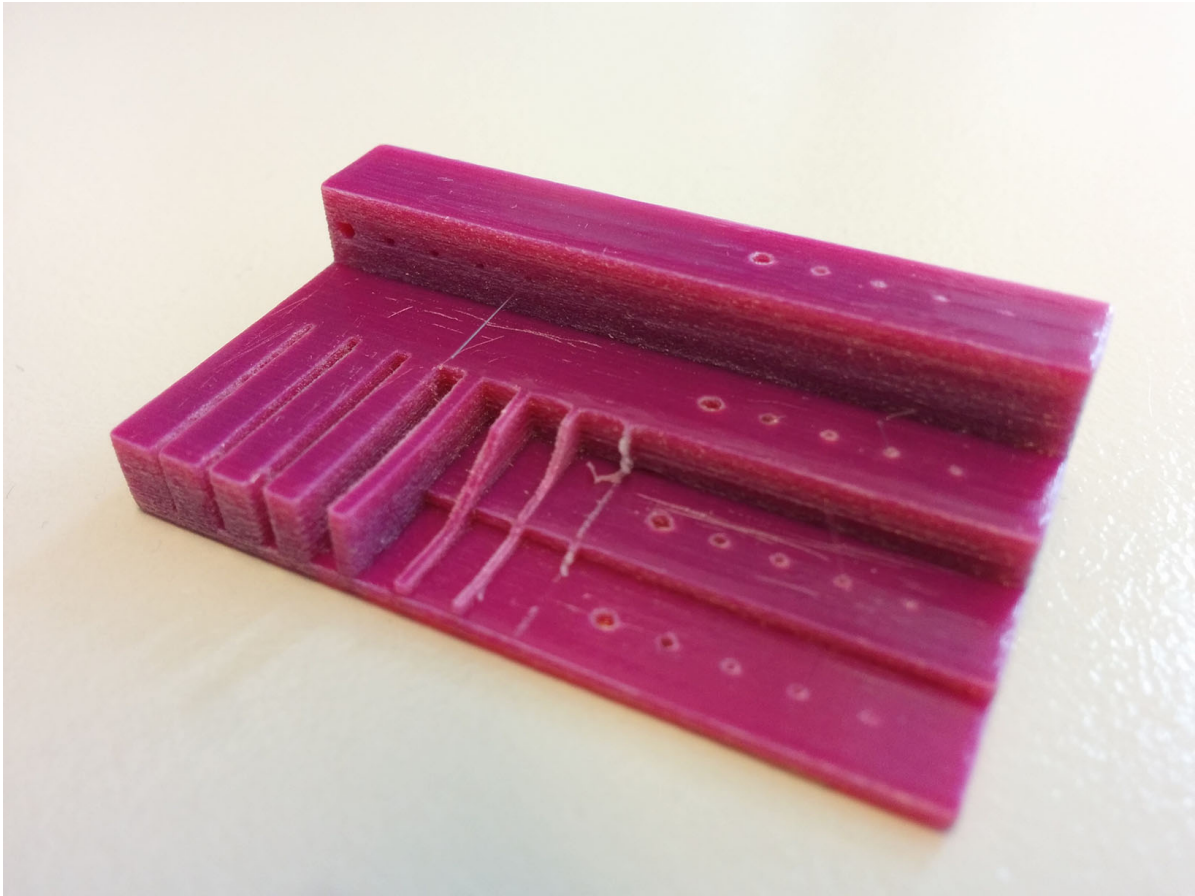


Figure 7.4: Printed model to test the minimal dimensions possible

together, a bayonet structure was chosen to create the connection between the two parts. Figure 7.5 shows the small bottom part of the electrode design, shown both from the bottom side, where the needles will be sticking out of, and the top side, showing the hollow structure. The diameter of this tube is 3 mm in total. The diameter of the bayonet legs in this first bayonet design is 500 μm . Since this turned out to be not quite stable, a second version with legs of 800 μm was made. This was stable, but still the handling turned out to be quite hard, so a final version with legs of 1200 μm was produced.

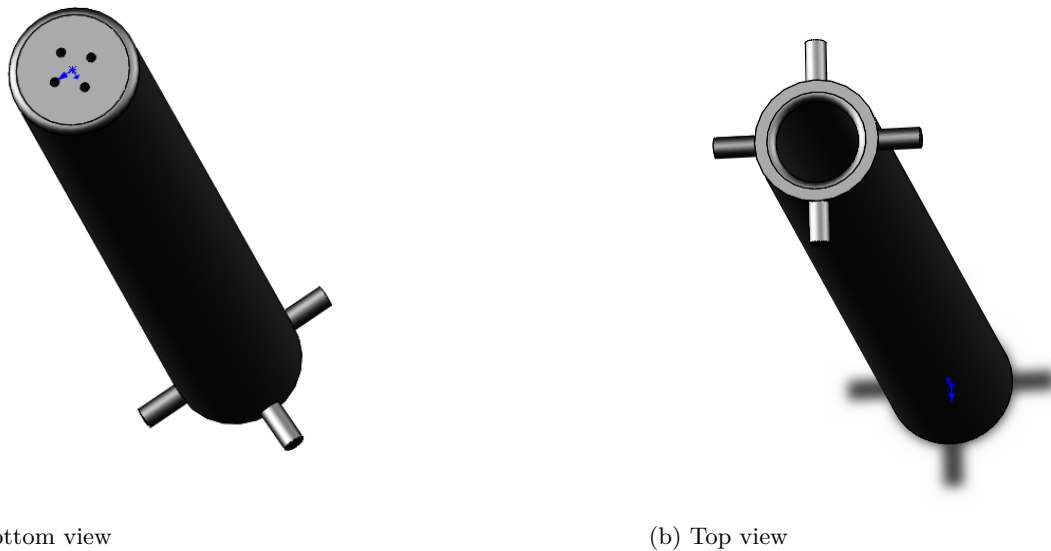


Figure 7.5: Small part of second 3D print electrode design

The other end of the bayonet electrode consists of a larger tube with slots to accept the extended parts of the small bottom part of the electrode. Figure 7.6 shows the design of this part. The bayonet parts of the design are going to make the connection between the two parts. The quartz will be removed from the tungsten needles at the connecting end of the bottom part. The conducting tungsten core of the needles will then be glued to the bayonet legs of this part by means of conducting glue. That way, the legs themselves will be conducting the signal from the needles to the top part, where the connection to regular cables takes place in a similar manner. Since the small bottom part was altered a few times with bigger bayonet legs, this design also went through multiple designs to be able to accept the small electrode part in the bayonet connection. The total diameter of this large tube is 13 mm.

The models were all created with the Connex3 Objet 350 printer from Stratasys. They were then cleaned using the process described in Subsection 7.2.2. The results are shown in Figures 7.7, 7.8 and 7.9. Figure 7.7 shows zoomed in photographs of the bottom and top view of the small part, as well as the bottom part of the big electrode part. Figure 7.8 shows both parts next to each other, both connected to each other and unconnected. Finally, Figure 7.9 shows the assembled versions. Both the needles in the small part and the cables in the top part are installed in the models. Only two needles can be seen in the small part. There actually are 4 needles present, but two needles are hidden behind the two visible needles.

7.4. Characterization

Since the only components in the signal path in this third electrode design are the tungsten needles, no further characterization is done. The rest of the connections are all made of relatively big conducting parts (such as a bayonet leg covered in conductive glue), so the impedance of these parts are considered to be negligible compared to the interface of the tungsten needles with the tissue (or saline solution). The impedance levels are analyzed in Chapter 6, Subsection 6.2. The levels found proved to be sufficient for the requirements that were set beforehand.

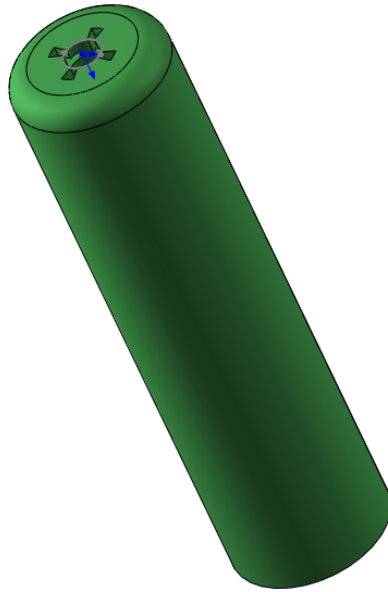
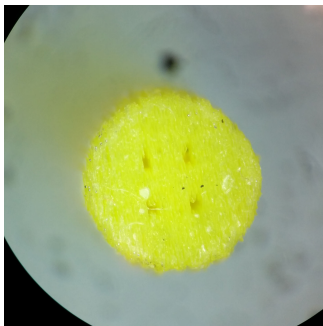


Figure 7.6: Bigger top part of the second 3D print electrode design



(a) Small part, bottom



(b) Small part, top



(c) Big part

Figure 7.7: Detailed images of the produced bayonet electrode

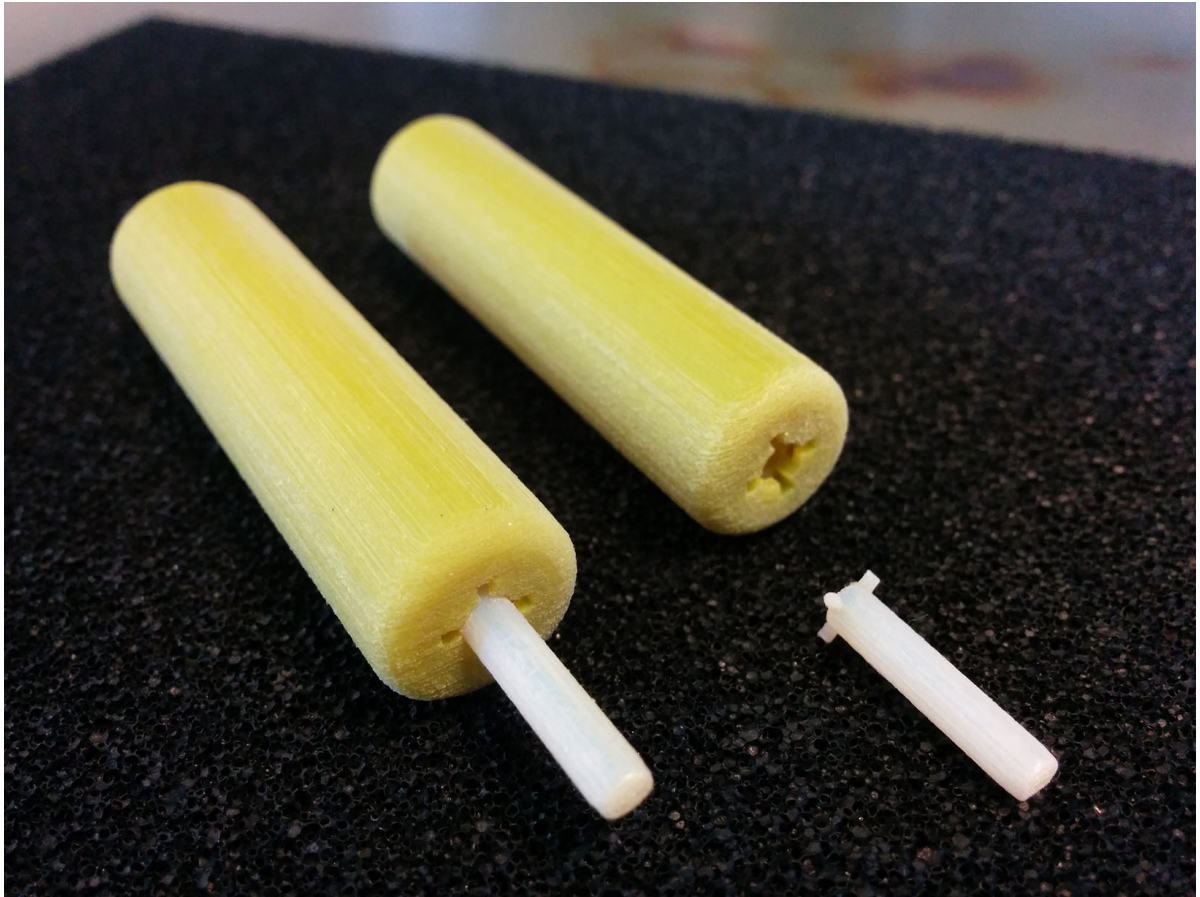


Figure 7.8: 3D printed bayonet electrode, both connected and unconnected



(a) Small part with needles



(b) Big part with cables

Figure 7.9: Assembled photographs of the bayonet electrode.

7.5. In vivo measurements

The 3D printed electrode was fully assembled and used to do in vivo measurements. The wires from the big end of the bayonet electrode were shortened and a connector was installed for easier use. A fully shielded cable was used to attach the electrode to the readout electronics to provide less interference from sources in the laboratory room. For the previous recordings, the electrode was hooked up to the Thomas Recording array, described in Subsection 3.2.2. For this measurement, a new readout system was used especially designed for this project. The next subsection shortly describes the improved setup (Subsection 7.5.1). The following subsections (7.5.2 and 7.5.3, respectively) give some of the results obtained when using the new electrode and new readout system in in vivo measurements.

7.5.1. Improved readout system

Since the ultimate goal of this project is to create a wearable system, a new readout system was designed by students simultaneously to the development of the new electrodes. This readout system contains amplifiers and analog-to-digital converters all in one small shielded box, so that future measurements don't need a big cage with a head stage anymore in order to do measurements. Furthermore, a micro-controller is present in the setup to adjust the settings in the amplifiers if needed and to obtain the recorded signal and store the signal onto an SD card. Since the system is built inside a metal box and all cables used are twisted pairs and shielded, there should be very little influence of external interference, as proven in earlier test measurements done with this system. More information about this readout system can be found in the thesis of this project [3].

7.5.2. Unfiltered data

The mouse was hooked up to the readout system described in Subsection 7.5.1 and the electrode was placed on top of the olivary tissue. Unfortunately, only one channel was recorded, since one of the needles broke during the final part of the assembly process. Although this is unfortunate (timing differences between locations can not be seen with only one channel), the proof of concept of the electrode can still prove valuable. The large part of the bayonet electrode turned out to be slightly too big to be held by a very precise micromanipulator, so a simpler clamp was used to attach the electrode and move it into place. Since the needles of the electrode are very fragile, this was a very suboptimal solution. Inspection of the electrode afterwards, however, showed very little damage to the needles, so no problems arose there. The depth at which the electrode was placed inside the tissue, did however prove to be a problem. More about this in Subsection 7.5.3

First of all, a measurement was started without the electrode hooked up to the readout system. During this measurement, the electrode was hooked up, and a clear change in recorded signal was observed, suggesting good connections between all the parts of the system. After this was established, a measurement of the olivary tissue activity was done. An excerpt of one of the measurements is given in Figure 7.10. This image shows the raw and unfiltered data obtained from the measurement. The same variety of frequency analysis figures are given in Figures 7.11 (for 0 to 2 kHz), 7.12 (for 0 to 200 Hz) and 7.13 (for 0 to 20 Hz).

The time domain data does show some oscillations present, but the nature of these oscillations doesn't seem to be animal activity, since the oscillations are in the order of 0.4 Hz. No known or anticipated signals inside the animal are in this frequency range, so most likely these oscillations are due to other sources around the measurement setup. Furthermore, in the frequency analysis a clear 50 Hz component can be seen. Although almost every part of the measurement setup is fully shielded against interference, this component is clearly not fully rejected by the system. An explanation for this might be that the animal itself wasn't properly grounded. The metal plate on which the mouse was placed was grounded, however via the Faraday cage in which the experiment took place, which in turn was grounded via earth, which clearly was contaminated by a 50 Hz component.

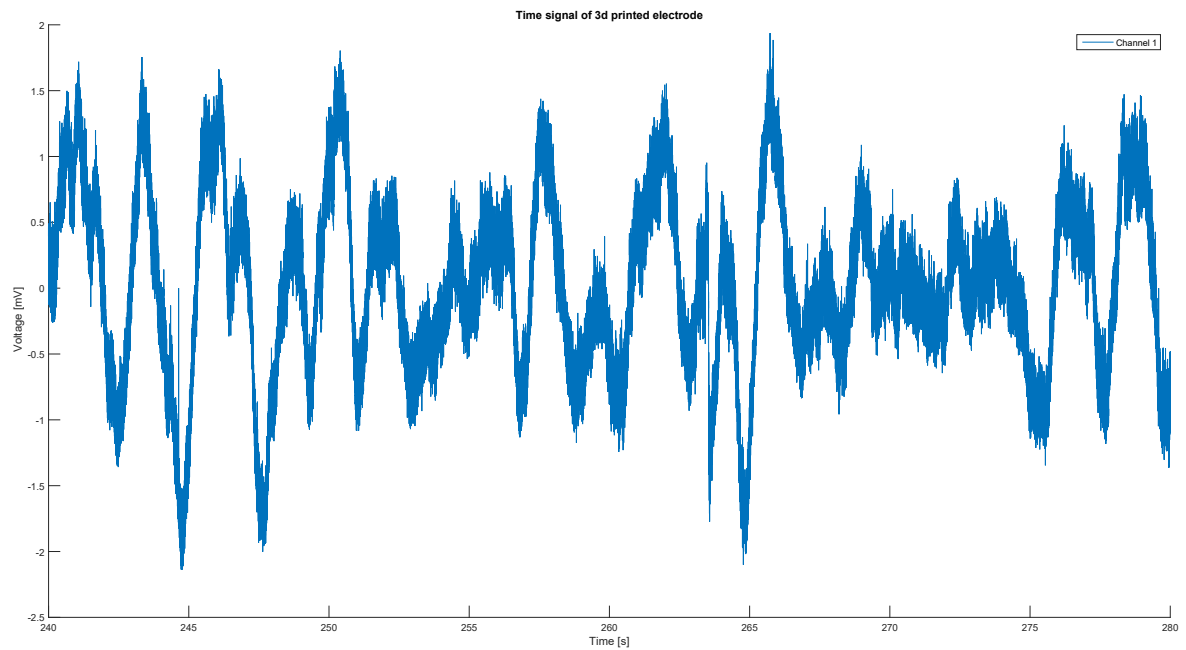


Figure 7.10: Excerpt of a raw time domain measurement with the 3D printed electrode design

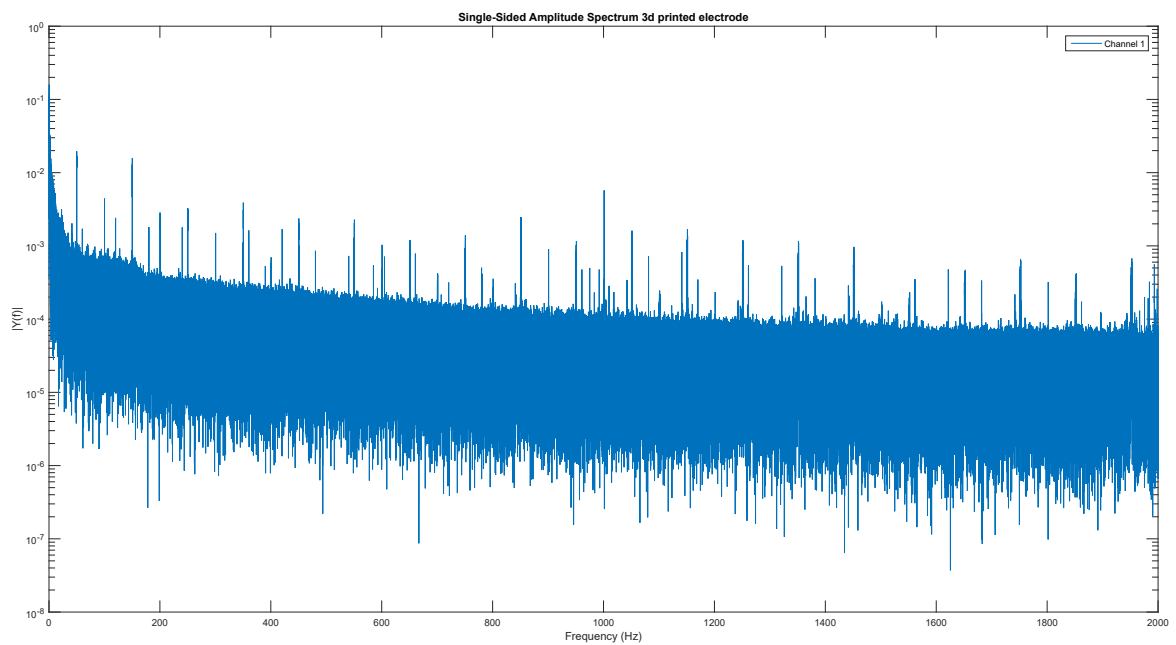


Figure 7.11: Frequency analysis of 3D printed design measurement, range 0 - 2 kHz

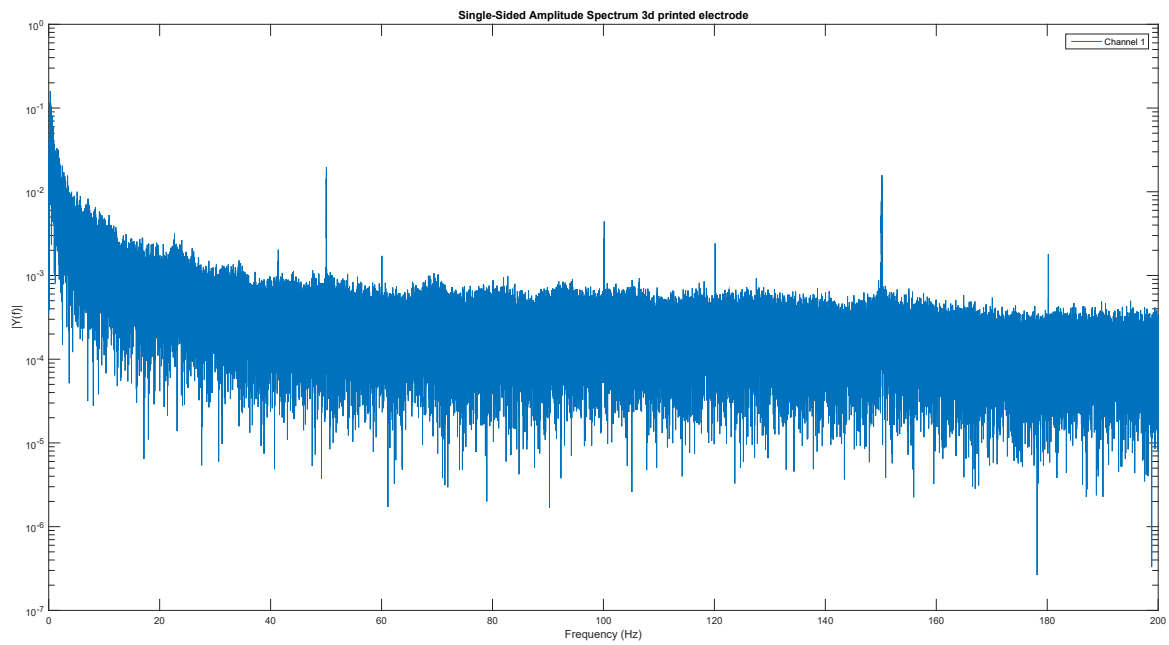


Figure 7.12: Frequency analysis of 3D printed design measurement, range 0 - 200 Hz

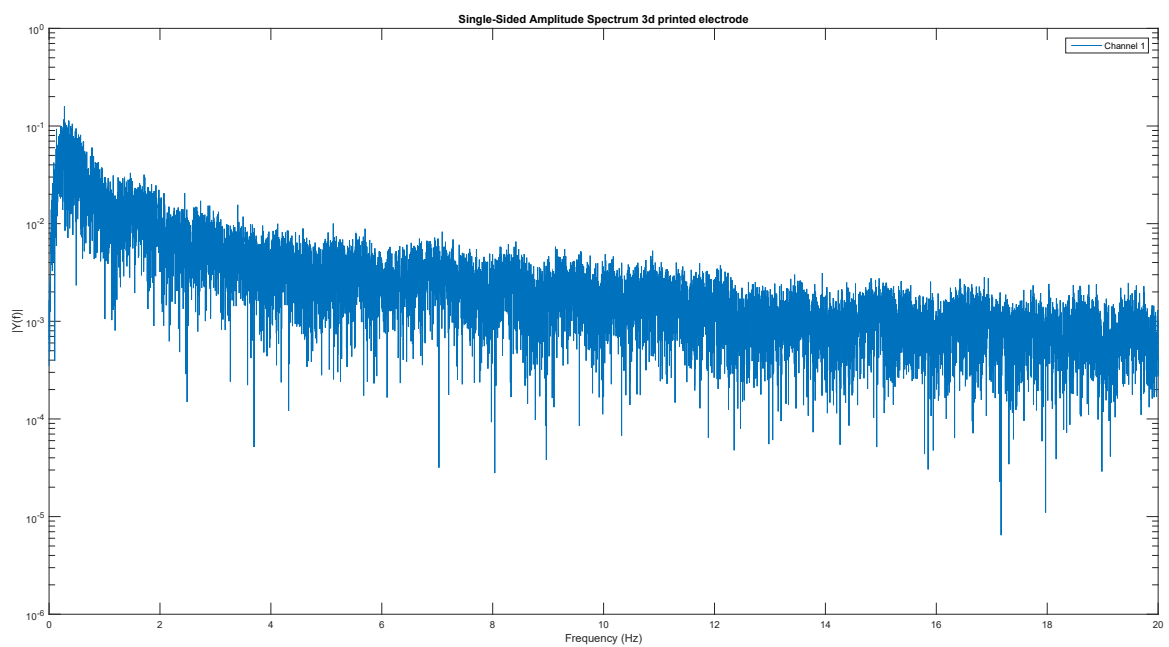


Figure 7.13: Frequency analysis of 3D printed design measurement, range 0 - 20 Hz

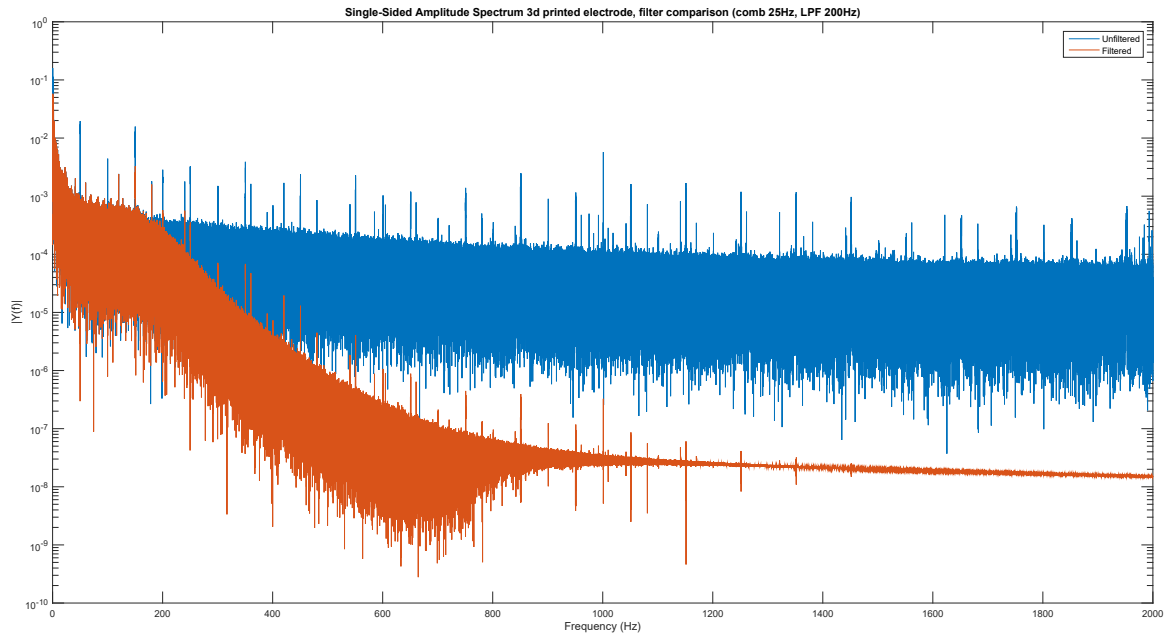


Figure 7.14: Comparison between unfiltered and filtered signal, frequency domain, range 0 - 2 kHz

7.5.3. Filtered data

To further investigate the information in the recording, the same filtering as used in Subsection 6.3.2 was applied: a comb filter with notches at 25 Hz and multiples of 25 Hz and a 6th order low pass Butterworth filter. Figures 7.14 and 7.15 show a comparison in the frequency domain between the unfiltered signal and the filtered signal, in the range of 0-2 kHz and 0-200 Hz, respectively. The effect of the filters can, as before, be clearly seen from these figures. In the filtered time domain data, however, still no expected signal is found (see Figure 7.16). The most likely explanation for this is that the placement of the electrode with the available clamp proved to be very hard, and chances are very real that the measuring tips of the system were either not deep enough into the tissue (thus floating in fluid above) or too deep inside (and through) the tissue, thus recording muscle activity, which is not present in this case since the animal was anesthetized. Although it is unfortunate that no real signal was recorded, the proof of concept for a 3D printed electrode design was still successful. Some modifications need to be made in the surrounding material rather than the electrode itself.

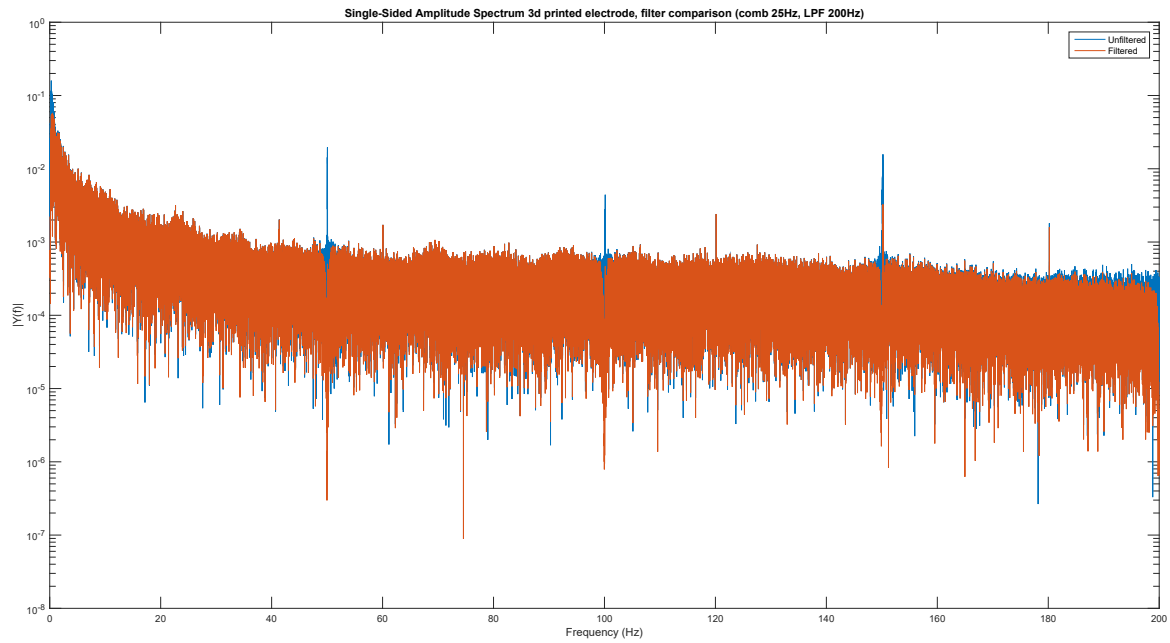


Figure 7.15: Comparison between unfiltered and filtered signal, frequency domain, range 0 - 200 Hz

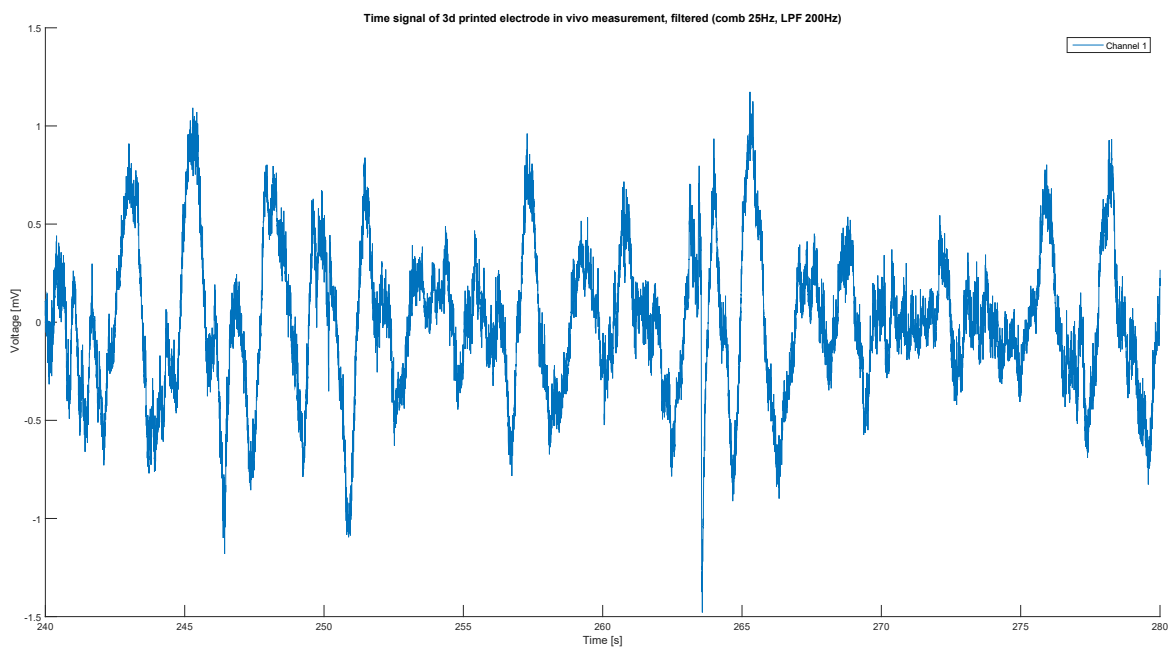
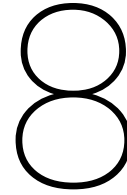


Figure 7.16: Filtered time domain data

7.6. Issues

Although a 3D printed electrode design has a lot of advantages compared to the first two designs and compared to the commercially available products, still some problems arose when designing and using the electrode.

- Most 3D printers have a resolution too big to be able to create structures this small, so a very high end 3D printer is needed to obtain such good results. Unfortunately, these printers are very expensive, and thus not available for small research projects.
- The scale doesn't only prove to be a problem in fabrication, the assembly of the electrode also proved to be very hard. Since the needles needed to be applied to the 3D printed structure, and these needles are very fragile, it is very hard to install all four needles without breaking one in the process. Although the method was chosen to be as easy as possible, still a lot of effort went into assembling the total electrode without breaking any of the structures.
- The spacing between the needles can be accurately designed by the 3D model, but since the needles are installed by hand, the length of the needles is still not very well controlled. Since it is important to know how deep the needles are in the tissue of the animal, this is a problem which needs to be solved before a real working solution is found.



Conclusions and recommendations

The research question for this project was formulated as: "*How can we use alternative production techniques to cheaply and reliably create structures for electrode arrays for in vivo multicell inferior olivary recordings?*". In order to come to an answer to this question three electrodes designs were made. The first design was made using FlexPCB techniques. The second design combined this technique with existing micro-electrodes. The third design used 3D printing techniques to create an electrode structure. This Chapter reflects back on the requirements set in Chapter 4 and discusses what goals are reached and what goals are not reached. This is done in Section 8.1. Since a lot of electrodes are already commercially available, Section 8.2 compares the newly designed electrodes with these products. Finally, Section 8.3 gives an overview of recommendations for future work.

8.1. Conclusions regarding requirements

In this section, the newly designed electrode configurations will be evaluated with respect to the requirements set in Chapter 4. Only the engineering requirements will be discussed, since these are based on the neuroscientific requirements, but viewed from an engineering point of view.

- **Material**

The FlexPCB material used in the first electrode design is a polyimide, which has been tested as a material suitable for chronic implantation [23]. The measuring spots were covered in gold, which is also an approved biocompatible material. The needles applied to the FlexPCB and later the 3D model are made of tungsten, which is marked as a biocompatible material [24]. They are insulated with a layer of quartz which is also used in a range of medical applications [25]. Since it is a glass material, there might be a risk of breaking and leaving shards of glass in the brain, so for chronic use, this Quartz insulator might not meet the requirements.

The 3D print material used for the models described in Chapter 7 is an ABS plastic, which is not marked as biocompatible, although it is not cytotoxic. The manufacturer of the 3D printer (Stratasys) does however offer a biocompatible print material, so a biomedical realization of the model could be realized, if the printer resolution would stay as was the case with ABS plastic.

- **Electrode size**

The first electrode design used gold droplets as electrode tips. These blobs have a diameter of about 50 μm , which does not meet the requirements for single cell recordings (tip < 20 μm). The second and third design used tungsten needles as electrode tips. These needles have a shaft diameter of 80 μm and a tip size of a few μm , so these do meet the requirements.

- **Array size**

All designs fit inside a triangle with sides of 3 mm, so all designs meet the requirement of not exceeding the dimensions of the olive.

- **Connection**

The first and second design were connected via a receptor board, which was made to be compatible

with the existing measuring setup in the laboratory. The third design was not compatible with this system, since a specialized readout system was designed during the project to which the third design was hooked up.

- **Impedance**

The impedance level of the first electrode design was very low since the measuring spots were relatively big (about 25 k Ω at 1 kHz). This design does meet the requirement, which stated that the impedance at 1 kHz should be below 5 M Ω . The second and third design included tungsten needles as measuring tips. Since these are a lot smaller, the impedance is a lot higher, but still the measured value of 1.5 M Ω meets the requirements. The needles do need to be grinded well, since the impedance goes up with a more blunt tip.

8.2. New electrodes compared to commercial electrodes

Although the newly designed electrodes perform well when using them, they still can't compete with the most advanced commercial products, such as the Utah Array (see Section 3.2). Using a 3D printer does however offer a lot of freedom when designing electrodes for specific applications. Every shape imaginable is possible, as long as the feature size of the design does not conflict with the resolution of the printer. Below, a few aspects are considered:

- **Size**

The printer used has a very high resolution, but the feature size still has a lower limit of about 100 μm . This is small enough to incorporate the tungsten needles, but is not yet small enough to do single cell measurements without the use of external components such as the tungsten needles. Commercially available products do offer smaller size electrodes.

- **Reproducibility**

The first electrode (FlexPCB) offers a great reproducibility, but the designs which require the tungsten needles to be installed do not. The length of the needles is adjusted by hand before fixating it, which does not guarantee the same length when a new electrode is assembled. To improve the reproducibility, a standardized process would be necessary. Besides that, the electrode tips are grinded by hand, which means that each electrode tip has a slightly different shape and a slightly different impedance along with that. These microwires are however a commercially available product, so the new electrode designs don't suffer from that more than the available products. Other products offer a pregrinded product, so reproducibility is higher in these cases.

- **Price**

The FlexPCB design is relatively expensive (about €70 a piece, without the addition of the gold semispheres). This price will go down if more are made in the same batch, since about half of this price consists of overhead costs such as tooling. The 3D printed design is very cheap (less than €1 each, not including the microwire tips). Such a design does however require a high resolution 3D printer, which was available for use during this project. These printers are very expensive and outsourcing this comes at a cost as well. Still, the created electrodes are very cheap compared to commercial products.

- **Robustness**

The robustness of the electrode designs are not yet good enough to compete with commercial products. The first design is fully made at a PCB manufacturer and is very robust, but both designs using the tungsten needles are very fragile since the Quartz insulator can easily break. This is especially the case when assembling the electrodes, so creating a more robust production method would be very beneficial for the robustness of the design. Besides that, the 3D print model needs to have a minimum dimension in order for the material to be stable enough. The first 3D model was created with too small features, resulting in a broken piece. The next design was adjusted for this issue and thus did not have this problem.

8.3. Recommendations

As discussed in Section 8.1 and 8.2, not all requirements have been met and not every aspect of the design is as desired. Below is a list of issues and recommendations that need to be investigated in order

for the design method to be effective.

- **Assembly**

Since both the second design and the third design require a manual assembly with very small and fragile parts, the reproducibility and robustness of the design are still not sufficient. Although the 3D structure itself is robust, it requires a production process in order to reliably create the electrodes.

- **Design**

The latest design, the 3D printed bayonet structure, gives a lot of freedom to researchers. The small part can be made in any shape (as long as there are no sharp bends, since the Quartz might break), so for any structure or tissue of interest the design can be altered for optimal placement. Besides, since the electrode consists of two parts, the small part can be replaced after use whereas the big part remains, cutting costs for the researchers. The design is however not yet ideal. The small part is hard to grab and therefore hard to use. The big part can be adjusted as well, in the end for example to create a wearable package. The big part might for example house some electronics or antennas to amplify and send the signal.

- **3D print material**

The current design is not made of biocompatible material, and is thus not suited for long term implantation. A biocompatible material is available, so the design could benefit from this change. This is however only possible if the biocompatible material offers at least the same resolution in printing.

Conducting print material would greatly increase the usefulness of a 3D printed electrode design. This way, the electrode can be made completely by machine and no further assembly is necessary. The bayonet legs could also be made with conductive material, creating a connector to the electronics. The current resolution of conductive material is not yet good enough to be beneficial in such a design (about 500 μm).

Bibliography

- [1] J. P. Allen, *The art of medicine in ancient Egypt*. Metropolitan Museum of Art, 2005.
- [2] A. P. Alivisatos, M. Chun, G. M. Church, R. J. Greenspan, M. L. Roukes, and R. Yuste, “The brain activity map project and the challenge of functional connectomics,” *Neuron*, vol. 74, no. 6, pp. 970–974, 2012.
- [3] M. Weskin, “A compact multi-electrode system to measure in vivo electrical activity in the olivo-cerebellar system,” Master’s thesis, Delft University of Technology, August 2016.
- [4] G. J. Tortora and B. H. Derrickson, *Principles of anatomy and physiology*. John Wiley & Sons, 2009.
- [5] J. C. Desclin, “Histological evidence supporting the inferior olive as the major source of cerebellar climbing fibers in the rat,” *Brain research*, vol. 77, no. 3, pp. 365–384, 1974.
- [6] R. E. Foster and B. E. Peterson, “The inferior olivary complex of guinea pig: cytoarchitecture and cellular morphology,” *Brain research bulletin*, vol. 17, no. 6, pp. 785–800, 1986.
- [7] R. S. van der Giessen, *Role of Electrotonic Coupling in the Olivocerebellar System*. Erasmus Universiteit Rotterdam, 2007.
- [8] P. D. Lampe and A. F. Lau, “Regulation of gap junctions by phosphorylation of connexins,” *Archives of biochemistry and biophysics*, vol. 384, no. 2, pp. 205–215, 2000.
- [9] P. D. Lampe and A. F. Lau, “The effects of connexin phosphorylation on gap junctional communication,” *The international journal of biochemistry & cell biology*, vol. 36, no. 7, pp. 1171–1186, 2004.
- [10] C. De Zeeuw, E. Hertzberg, and E. Mugnaini, “The dendritic lamellar body: a new neuronal organelle putatively associated with dendrodendritic gap junctions,” *The Journal of neuroscience*, vol. 15, no. 2, pp. 1587–1604, 1995.
- [11] L. M. Davis, M. E. Rodefeld, K. Green, E. C. Beyer, and J. E. Saffitz, “Gap junction protein phenotypes of the human heart and conduction system,” *Journal of cardiovascular electrophysiology*, vol. 6, no. 10, pp. 813–822, 1995.
- [12] T. Liu, D. Xu, J. Ashe, and K. Bushara, “Specificity of inferior olive response to stimulus timing,” *Journal of Neurophysiology*, vol. 100, no. 3, pp. 1557–1561, 2008.
- [13] D. Xu, T. Liu, J. Ashe, and K. O. Bushara, “Role of the olivo-cerebellar system in timing,” *The Journal of Neuroscience*, vol. 26, no. 22, pp. 5990–5995, 2006.
- [14] V. Giagka, *Flexible Active Electrode Arrays For Epidural Spinal Cord Stimulation*. PhD thesis, UCL (University College London), 2015.
- [15] S. F. Cogan, “Neural stimulation and recording electrodes,” *Annu. Rev. Biomed. Eng.*, vol. 10, pp. 275–309, 2008.
- [16] MicroProbes, “Microprobes single electrodes,” 2016. <https://www.microprobes.com/index.php/products/metal-microelectrodes/single-electrodes>.
- [17] ThomasRecording, “Thomas recording single electrodes,” 2016. <http://www.thomasrecording.com/neuroscience-products/metal-microelectrodes/single-electrodes/>.
- [18] P. Salvo, R. Raedt, E. Carrette, D. Schaubroeck, J. Vanfleteren, and L. Cardon, “A 3d printed dry electrode for ecg/eeG recording,” *Sensors and Actuators A: Physical*, vol. 174, pp. 96–102, 2012.

- [19] T. F. Scientific, “Pbs (10x), ph 7.4 - thermo fisher scientific,” 2016. <https://www.thermofisher.com/order/catalog/product/70011051>.
- [20] J. Gehrmann, P. E. Hammer, C. T. Maguire, H. Wakimoto, J. K. Triedman, and C. I. Berul, “Phenotypic screening for heart rate variability in the mouse,” *American Journal of Physiology-Heart and Circulatory Physiology*, vol. 279, no. 2, pp. H733–H740, 2000.
- [21] A. J. Ewald, Z. Werb, and M. Egeblad, “Monitoring of vital signs for long-term survival of mice under anesthesia,” *Cold Spring Harbor protocols*, vol. 2011, no. 2, pp. pdb-prot5563, 2011.
- [22] Stratasys, “Stratasys objet350 connex3 specifications,” 2016. <http://www.stratasys.com/3d-printers/production-series/connex3-systems>.
- [23] B. Rubehn and T. Stieglitz, “In vitro evaluation of the long-term stability of polyimide as a material for neural implants,” *Biomaterials*, vol. 31, no. 13, pp. 3449–3458, 2010.
- [24] M. Peuster, C. Fink, and C. von Schnakenburg, “Biocompatibility of corroding tungsten coils: in vitro assessment of degradation kinetics and cytotoxicity on human cells,” *Biomaterials*, vol. 24, no. 22, pp. 4057–4061, 2003.
- [25] L. L. Hench and J. Wilson, “Biocompatibility of silicates for medical use,” *Silicon Biochemistry*, pp. 231–246, 1986.